

Congratulations for 70th Anniversary

of

Turkish Physical Society

and

Korean Physical Society

*We enjoyed 2002 World Cup Semi-final Match
(Turkiye 3 : 2 Korea)*

And

*Korea thanks Turkish Army for one of 16-UN Forces
during Korean Conflict in 1950-1953*

Brief Facts about Korea



People & Language: Korean (~4,500 yrs in the area)

Area (South): ~100,000 km² (~38,000 sq. mi.)

Population (South): 52 million

Recent History:

1945: Divided into North and South

1950~1953: Korean Conflict

1960~1970: Modernization (Migration to cities)

1970~1980: Industrialization (Heavy Industries)

1990~2022: High-tech oriented

Leading Industries:

Electronics, Automobile, Ship-building,
Steel, Chemicals, Construction

Economy: GDP = 1.8 T\$ and 35.4 k\$/capita in 2021

Religion: Christian (~30%), Buddhism (~30%)

Education: > 80% high-school seniors go to college

Accelerator Facilities in Korea (2022)



4GSR Project (KPS)
(Under construction)



Rare Isotope Science Project (RISP)
(Under construction)



PAL-XFEL (10.0 GeV) and
PLS-II (3.0 GeV Light Source)



KOMAC (100-MeV Proton Linac)

*Status and Prospects
of
Pohang Accelerator Laboratory (PAL)*

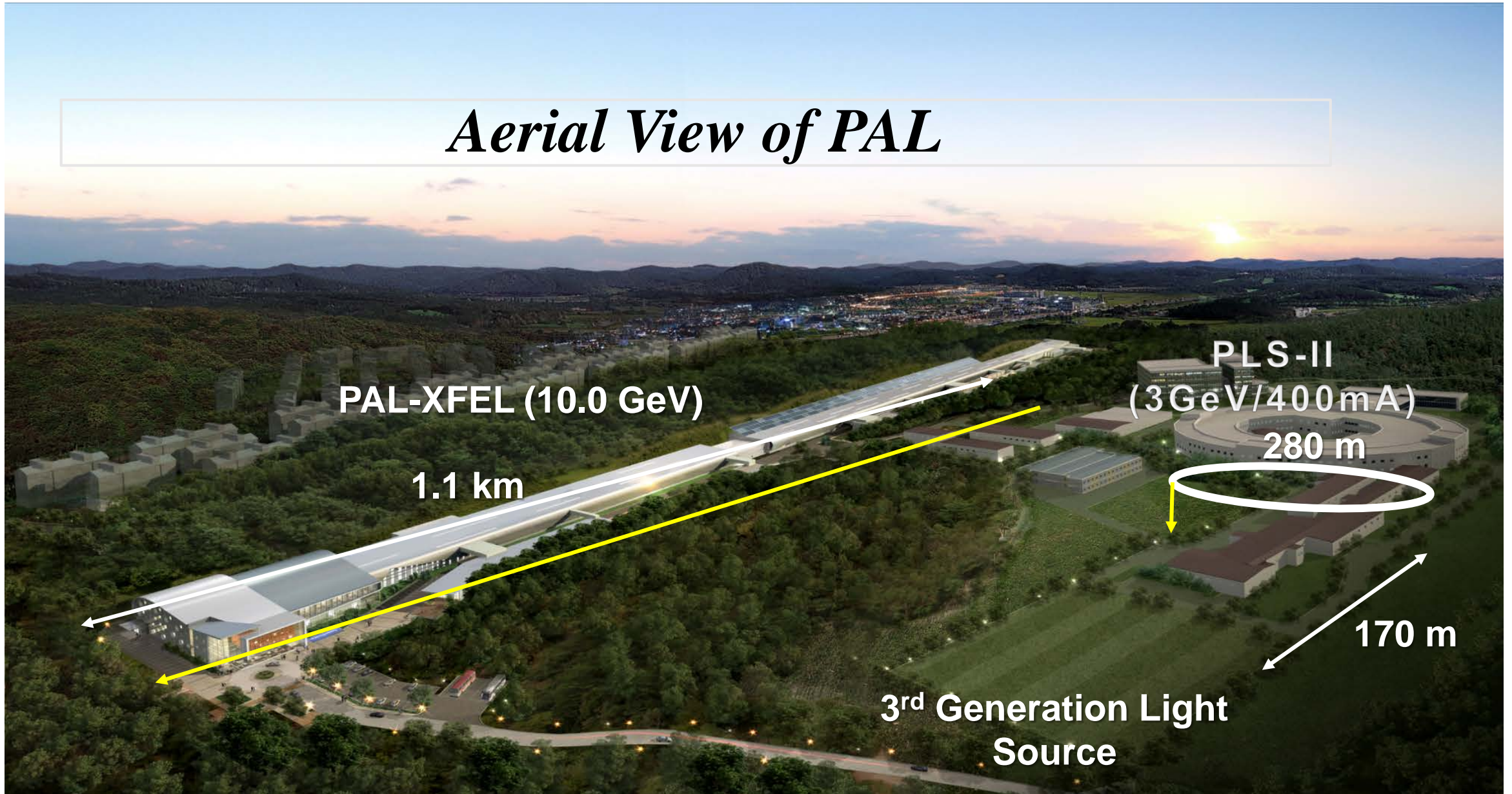
UPHUK-VIII
Bodrum, Turkiye

September 5-7, 2022

Won Namkung

PAL, POSTECH

Aerial View of PAL



Pohang Accelerator Laboratory Overview

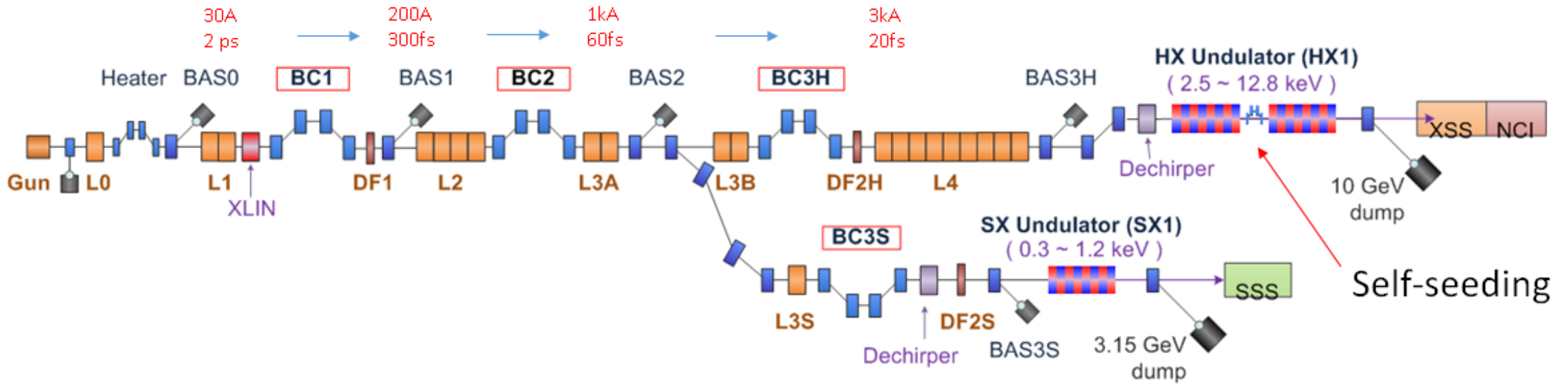
- *POSTECH*, a newly established university, proposed to construct a synchrotron light source on its campus in 1988
- *PLS is a 3rd generation synchrotron radiation source:*
 - 2 GeV injector linac and storage ring with upgrade option to 2.5-GeV
 - Construction Project: April 1988 ~ December 1994
 - Funded by POSCO (60%) & Government (40%)
- *Upgraded to 3.0 GeV in 2011 (PLS-II)*
- *PAL-XFEL (X-ray Free Electron Laser) was constructed in 2015*
 - World 3rd after SLAC (US) and SACLA (Japan)
- PAL is donated to Government in 2018
- *KPS Project (4.0 GeV, 4GSR) is started with KBSI in Chung-ju (2021-2027)*

PAL-XFEL

Initial proposal was to use existing PLS linac
to be a leading group member in 2003

Revised proposal in 2010 for 10 GeV XFEL

PAL-XFEL Layout and Parameters

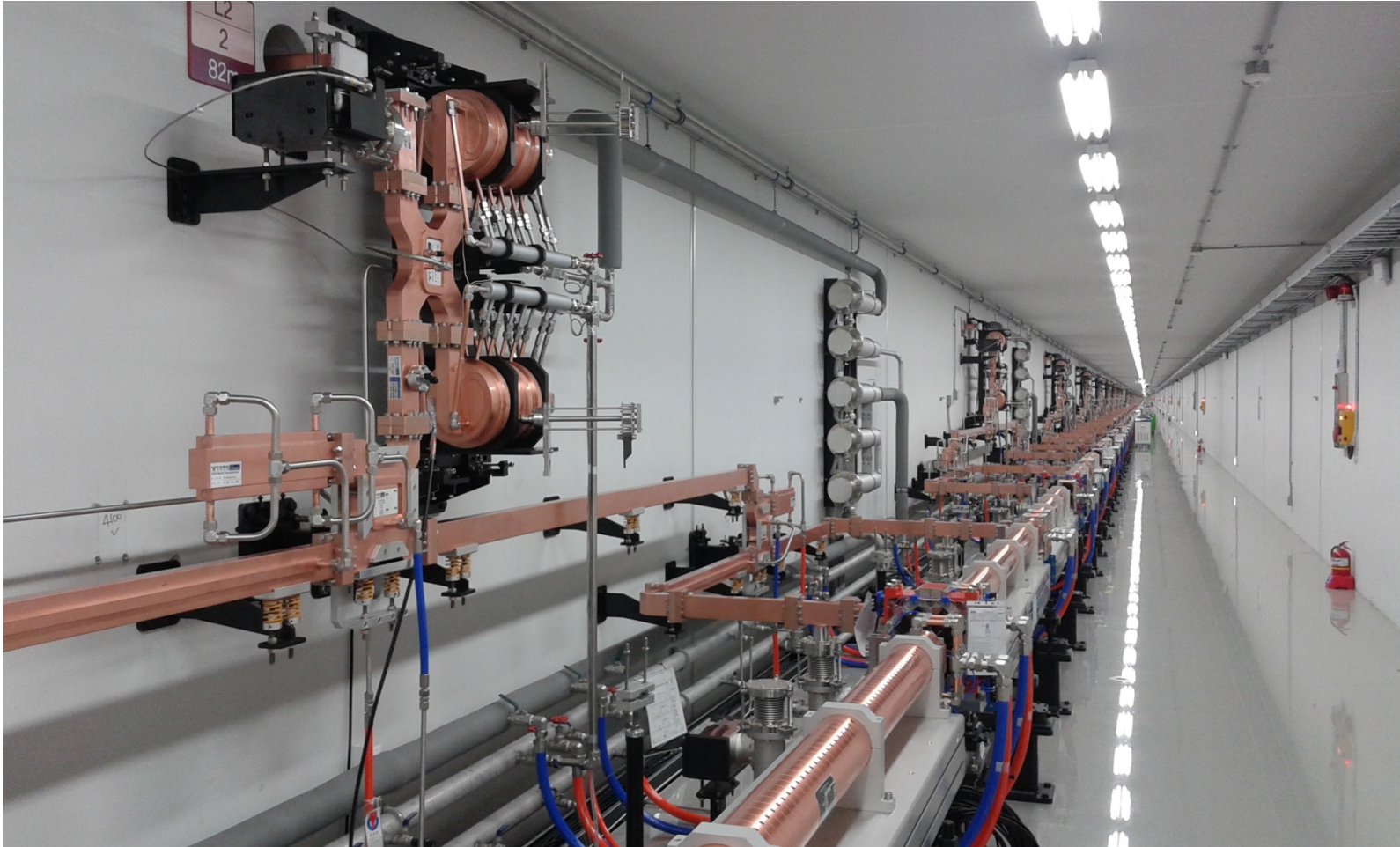


Main parameters

e^- Energy	10 GeV
e^- Bunch charge	20-200 pC
Slice emittance	< 0.4 mm mrad
Repetition rate	60 Hz
Bunch length	5 fs – 50 fs
Peak current	3 kA
SX line switching	Kicker Magnet

Undulator Line	HX	SX
Photon energy [keV]	2.4 ~ 15	0.28 ~ 1.0
Beam Energy [GeV]	4 ~ 11	3.0
Wavelength Tuning	Energy	Gap
Undulator Type	Planar	Planar
Undulator Period / Gap [mm]	26 / 8.3	35 / 9.0

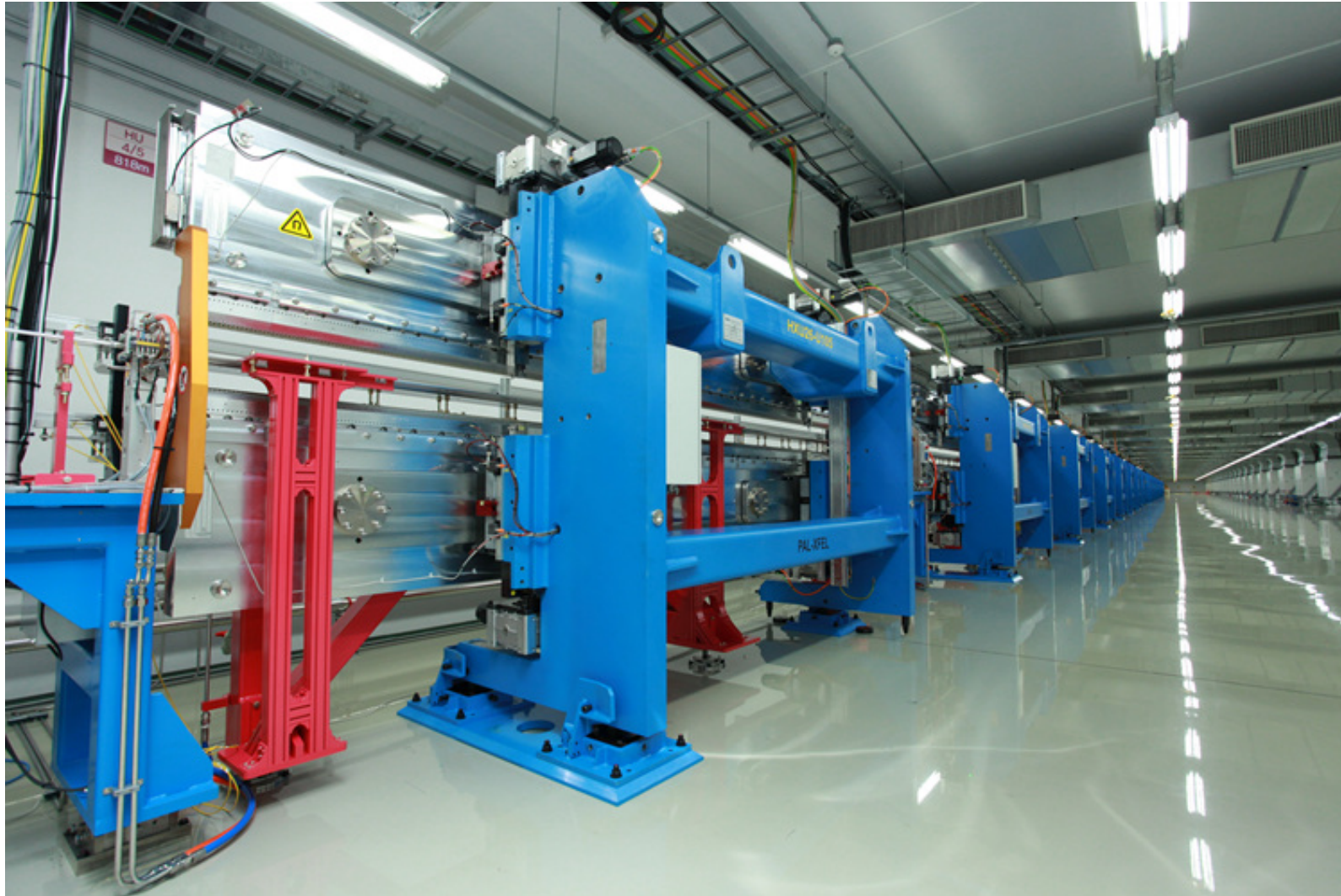
Linac Tunnel



Cross Section of Acceleration. Column

Parameter	Unit	Value
Energy	GeV	10
Charge	pC	200
No. of SLED		42
No. of Acc. Column		173

Undulator Hall

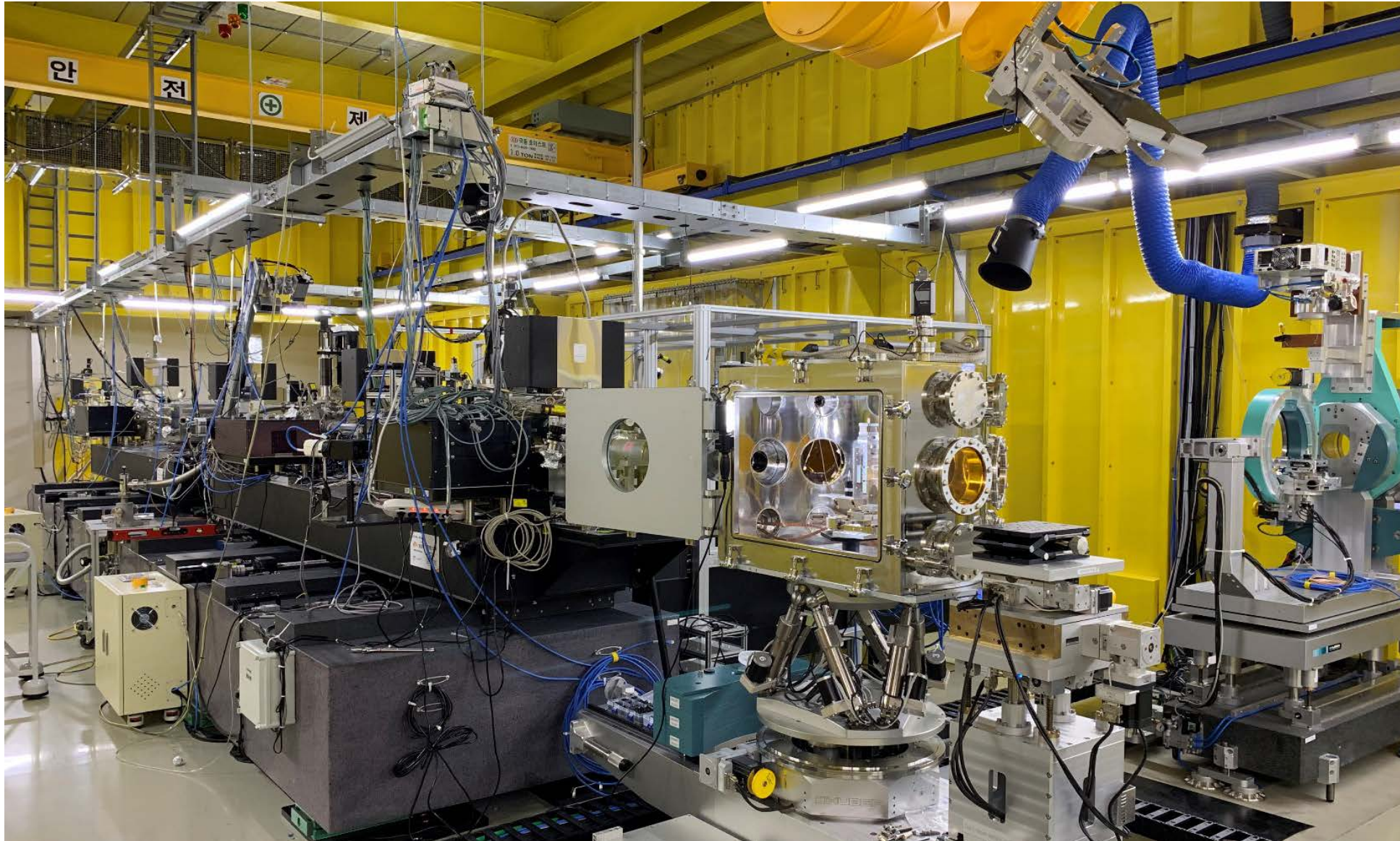


Parameter	Unit	Value
No. of Undulator		21
Length	m	5
Period	mm	26.0
Gap	mm	8.3
Wavelength	nm	0.1
Magnetic field	Tesla	0.8124
K		1.9727

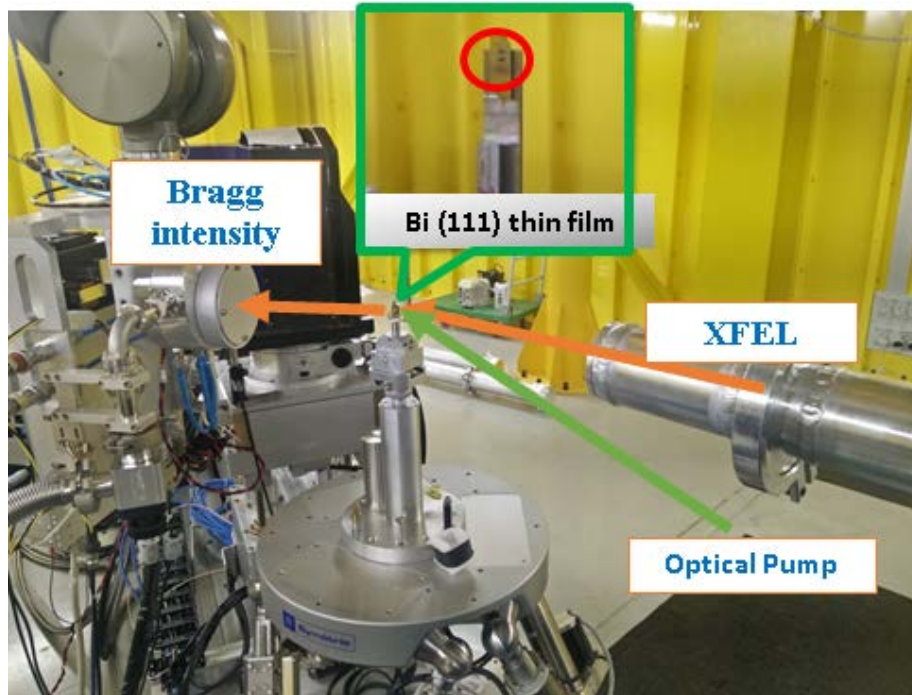
Hard X-ray Experiment Hutches



Hard X-ray Experiment Station

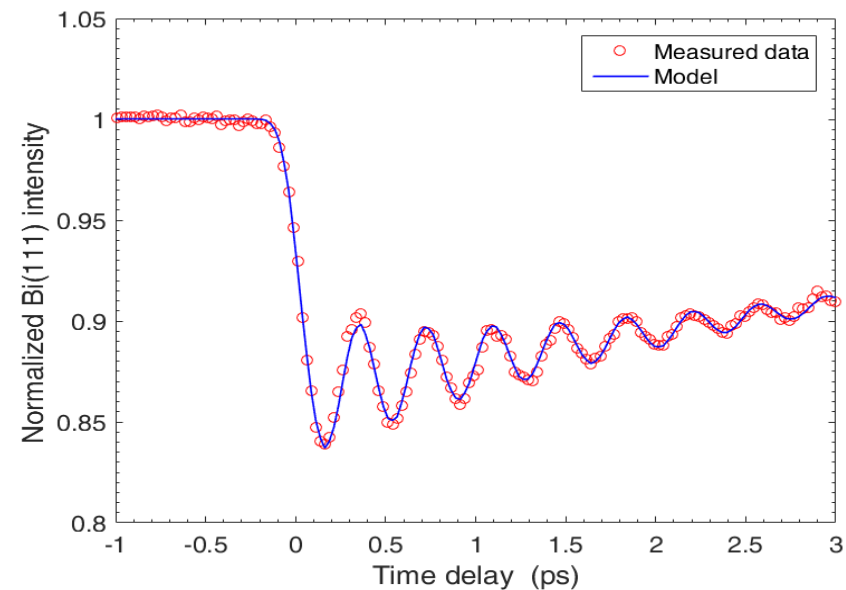


Hard X-ray FEL with Femtosecond Timing Jitter

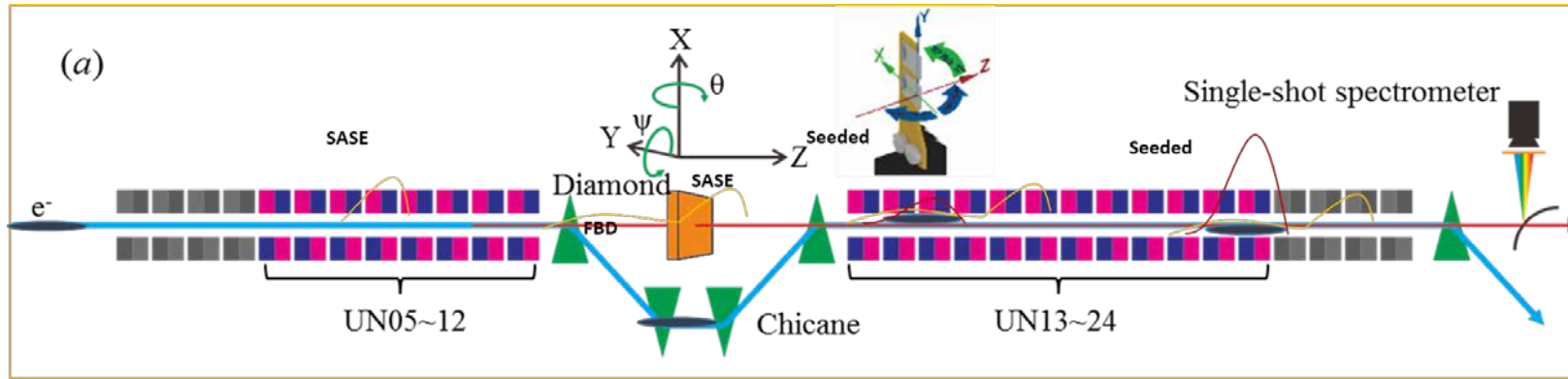


Bi(111) thin film (50 nm) on GaSb(111)/Si(111)
X-ray: 6 keV
X-ray size: $\sim 60 \times 60 \text{ um}^2$
Laser: 800 nm, 100 fs
Detector: MPCCD 0.5M

- No timing jitter correction
- averaged by 50 trials of the time delay scan and normalized by GaSb(111) Bragg peak intensity
- Only slow time-drift correction
- Vibration Frequency : 2.7 THz
- Instrument Response: 137 fs (FWHM)



Hard X-ray self seeding



- $E_c = 9.7 \text{ keV}$
- SASE bandwidth (FWHM) = 27 eV
- Self-seeding bandwidth (FWHM) = 0.22 eV
- Averaged pulse energy: $\sim 850 \mu\text{J}$
- FEL Pulse duration = $\sim 20 \text{ fs}$

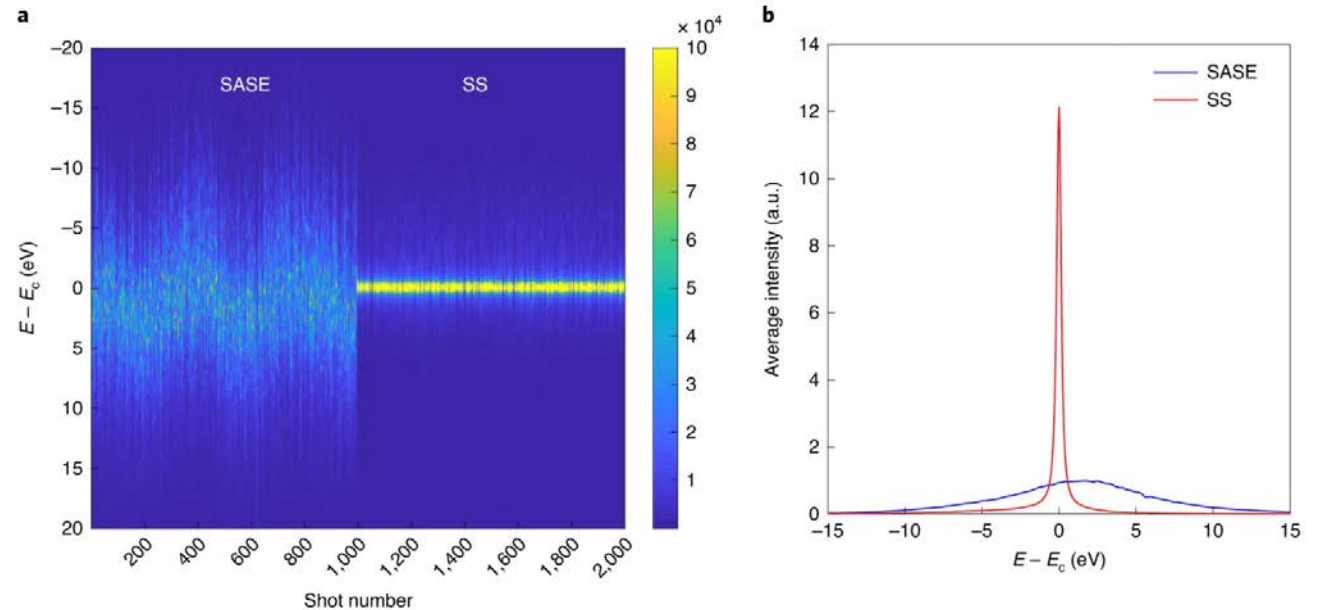


High-brightness self-seeded X-ray free-electron laser covering the 3.5 keV to 14.6 keV range

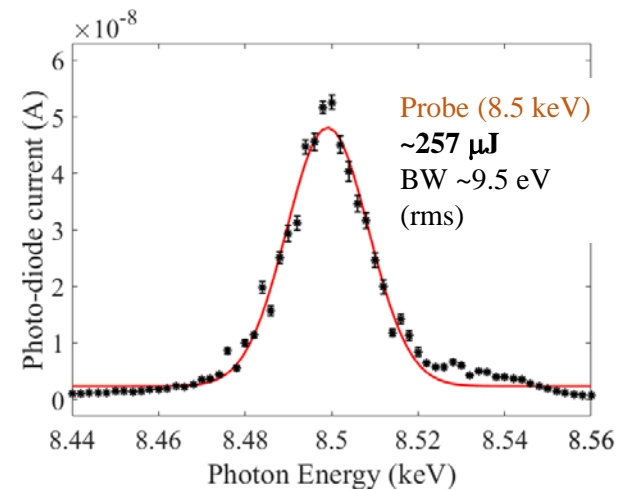
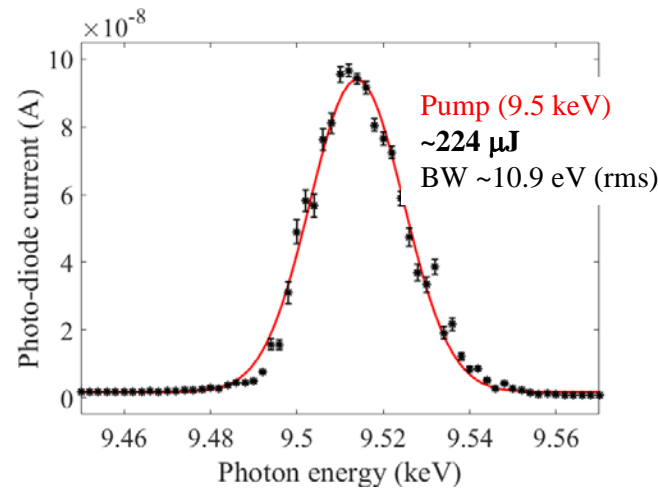
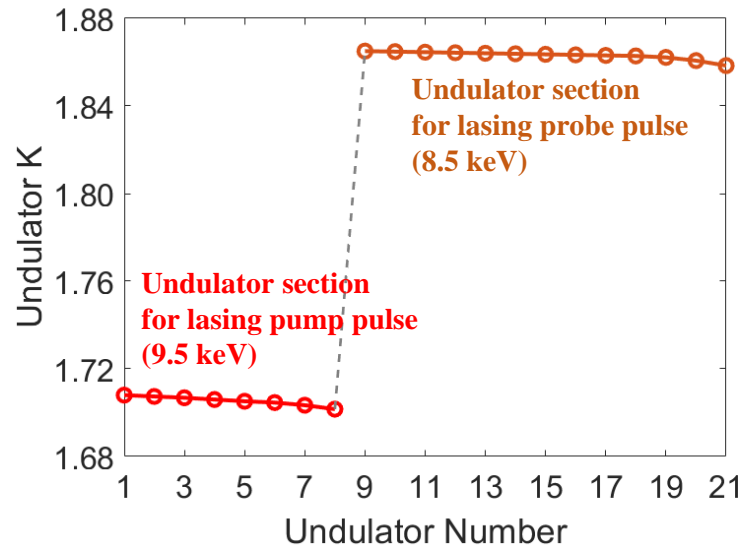
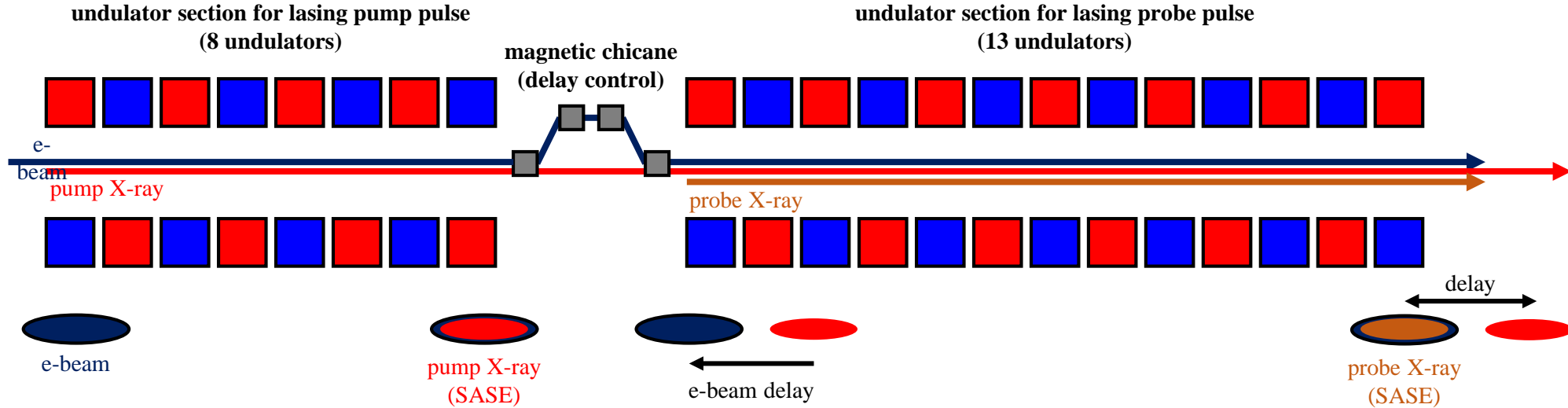
Inhyuk Nam^{1,4}, Chang-Ki Min^{1,4}, Bonggi Oh^{1,4}, Gyujin Kim¹, Donghyun Na¹, Young Jin Suh¹, Haeryong Yang¹, Myung Hoon Cho¹, Changbum Kim¹, Min-Jae Kim¹, Chi Hyun Shim¹, Jun Ho Ko¹, Hoon Heo¹, Jaehyun Park¹, Jangwoo Kim¹, Sehan Park¹, Gisu Park¹, Seonghan Kim¹, Sae Hwan Chun¹, HyoJung Hyun¹, Jae Hyuk Lee¹, Kyung Sook Kim¹, Intae Eom¹, Seungyu Rah¹, Deming Shu², Kwang-Je Kim², Sergey Terentyev³, Vladimir Blank³, Yuri Shvyd'ko^{2,3}, Sang Jae Lee^{1,3} and Heung-Sik Kang^{1,3}

A self-seeded X-ray free-electron laser (XFEL) is a promising approach to realize bright, fully coherent free-electron laser (FEL) sources in the hard X-ray domain that have been a long-standing issue with longitudinal coherence remaining challenging. At the Pohang Accelerator Laboratory XFEL, we have demonstrated a hard X-ray self-seeded XFEL with a peak brightness of $3.2 \times 10^{35} \text{ photons s}^{-1} \text{ mm}^{-2} \text{ mrad}^{-2} 0.1\% \text{ BW}^{-1}$ at 9.7 keV. The bandwidth (0.19 eV) is about 1/70 times as wide (close to the Fourier transform limit) and the peak spectral brightness is 40 times higher than in self-amplified spontaneous emission (SASE), with substantial improvements in the stability of self-seeding and noticeably suppressed pedestal effects. We could reach an excellent self-seeding performance at a photon energy of 3.5 keV (lowest) and 14.6 keV (highest) with the same stability as the 9.7 keV self-seeding. The bandwidth of the 14.6 keV seeded FEL was 0.32 eV, and the peak brightness was $1.3 \times 10^{35} \text{ photons s}^{-1} \text{ mm}^{-2} \text{ mrad}^{-2} 0.1\% \text{ BW}^{-1}$. We show that the use of seeded FEL pulses with higher reproducibility and a cleaner spectrum results in serial femtosecond crystallography data of superior quality compared with data collected using SASE mode.

Nat. Photon. **15**, 435 (2021)



Two-color HX FEL pulse generation



Machine study results (2022. 01. 15)

PAL-XFEL Machine Performance

FEL position stability:	< 10 % of beam size
FEL power stability:	< 5 % rms
E-beam energy jitter:	< 0.015 %
E-beam arrival time jitter:	< 15 fs
FEL pulse energy:	> 3.18 mJ at 7.13 keV
FEL beam pulse duration:	20 ~ 30 fs (FWHM)
Saturated FEL:	up to 20.0 keV

- Lattice design used three bunch compressor configuration
- Machine stability is outstanding
- Self-seeding and two-color generation are very promising

PAL-XFEL Statistics

Annual Plan of Operation (Days)

	2017	2018	2019	2020	2021	2022
User Beam-time	120	140	160	170	180	190
Turn-on & Tuning	123	110	73	67	70	57
Machine Study			21	21	10	10
Maintenance	109	102	98	97	92	95

User Service

	Applied	Approved	Days of Service
2017	82	26	120
2018	84	45	140
2019	140	49	160
2020	118	51	170
2021	132	47	180
2022	131	53	190

Maxima in the thermodynamic response and correlation functions of deeply supercooled water

Kyung Hwan Kim,^{1,*} Alexander Späh,^{1,4} Harshad Pathak,¹ Fivos Perakis,¹ Daniel Mariedal,¹ Sangsoo Kim,³ J

WATER PHASES

Experimental observation of the liquid-liquid transition in bulk supercooled water under pressure

Kyung Hwan Kim^{1,2,*}, Katrin Amann-Winkel^{1,4}, Nicolas Giovambattista^{3,4}, Alexander Späh¹, Fivos Perakis¹, Harshad Pathak¹, Marjorie Ladd Parada¹, Cheolhee Yang², Daniel Mariedahl¹, Tobias Eklund¹, Thomas. J. Lane^{5,6}, Seonju You², Sangmin Jeong², Matthew Weston¹, Jae Hyuk Lee⁷, Intae Eom⁷, Minseok Kim⁷, Jaeku Park⁷, Sae Hwan Chun⁷, Peter H. Poole⁸, Anders Nilsson^{1,†}

SCIENCE ADVANCES | RESEARCH ARTICLE

APPLIED SCIENCES AND ENGINEERING

Ultrafast x-ray diffraction study of melt-front dynamics in polycrystalline thin films

Tadesse A. Assefa^{1,*}, Yue Cao^{1,†}, Soham Banerjee^{1,2}, Sungwon Kim³, Dongjin Kim³, Heemin Lee⁴, Sunam Kim⁵, Jae Hyuk Lee⁵, Sang-Youn Park⁵, Intae Eom⁵, Jaeku Park⁵, Daewoog Nam⁵, Sangsoo Kim⁵, Sae Hwan Chun⁵, Hyojung Hyun⁵, Kyung sook Kim⁵, Pavol Juhas⁶, Emil S. Bozin¹, Ming Lu⁷, Changyong Song⁴, Hyunjung Kim³, Simon J. L. Billinge^{1,2}, Ian K. Robinson^{1,8*}

SCIENCE ADVANCES | RESEARCH ARTICLE

MATERIALS SCIENCE

Subnanosecond phase transition dynamics in laser-shocked iron

H. Hwang¹, E. Galtier², H. Cynn³, I. Eom⁴, S. H. Chun⁴, Y. Bang¹, G. C. Hwang¹, J. Choi¹, T. Kim¹, M. Kong¹, S. Kwon¹, K. Kang¹, H. J. Lee², C. Park⁵, J. I. Lee⁵, Yongmoon Lee⁶, W. Yang⁶, S.-H. Shim⁷, T. Vogt⁸, Sangsoo Kim⁴, J. Park⁴, Sunam Kim⁴, D. Nam⁴, J. H. Lee⁴, H. Hyun⁴, T.-Y. Koo⁴, C.-C. Kao², T. Sekine^{6,9}, Yongjae Lee^{1,6,*}

Article

Mapping the emergence of molecular vibrations mediating bond formation

https://doi.org/10.1038/s41586-020-2417-3
Received: 18 October 2019
Accepted: 16 April 2020
Published online: 24 June 2020
Check for updates

Jong Goo Kim^{1,2}, Shunsuke Nozawa^{4,5}, Hanul Kim^{1,2,3}, Eun Hyuk Choi^{1,2,3}, Tokushi Sato^{6,7}, Tae Wu Kim^{1,2,3}, Kyung Hwan Kim¹, Hosung Ki^{1,2,3}, Jungmin Kim^{1,2,3}, Minseo Cho^{1,2,3}, Yunbeom Lee^{1,3}, Jun Heo^{1,3}, Key Young Oang¹, Kouhei Ichihara^{6,7}, Ryo Fukaya⁶, Jae Hyuk Lee⁸, Jaeku Park⁸, Intae Eom⁸, Sae Hwan Chun⁸, Sunam Kim⁹, Minseok Kim⁹, Tetsuo Katayama¹⁰, Tadashi Togauchi¹¹, Sigeki Owada¹², Makina Tabuchi¹³, Sang Jin Lee^{1,2,3}, Seonggon Lee^{1,2,3}, Chi Woo Ahn^{1,2}, Doo-Sik Ahn^{1,2}, Jwon Moon³, Seungjoo Choi^{1,2}, Joonghan Kim¹, Talha Joo⁴, Jeongho Kim⁴, Shin-ichi Adachi^{1,4} & Hyotcherl Ihee^{1,2,3,22}

Won Namkung

High-Throughput 3D Ensemble Characterization of Individual Core–Shell Nanoparticles with X-ray Free Electron Laser Single-Particle Imaging

Do Hyung Cho,^{1,▽} Zhou Shen,^{1,▽} Yungok Ihm, Dae Han Wi, Chulho Jung, Daewoong Nam, Sangsoo Kim, Sang-Youn Park, Kyung Sook Kim, Daeho Sung, Heemin Lee, Jae-Yong Shin, Junha Hwang, Sung Yun Lee, Su Yong Lee, Sang Woo Han, Do Young Noh, N. Duane Loh,* and Changyong Song*

PHYSICAL REVIEW X 11, 031031 (2021)

Structural Evidence for Ultrafast Polarization Rotation in Ferroelectric Superlattice Nanodomains

Hyeon Jun Lee,¹ Youngjun Ahn,¹ Samuel D. Marks,*¹ Eric C. Landahl,² Shihao Zhuang,¹ M Matthew Dawber,³ Jun Young Lee,⁴ Tae Yeon Kim,⁴ Sanjith Unithrattil,⁴ Sae Hwan Chun,*⁵ Sun Sang-Yeon Park,*⁵ Kyung Sook Kim,⁵ Soohyeong Lee,^{6,7} Ji Young Jo,*⁴ Jiamian Hu,*¹ and

Optical Kerr Effect of Liquid Acetonitrile Probed by Femtosecond Time-Resolved X-ray Liquidography

Hosung Ki,[▽] Seungjoo Choi,[▽] Jungmin Kim, Eun Hyuk Choi, Seonggon Lee, Yunbeom Lee, Kihwan Yoon, Chi Woo Ahn, Doo-Sik Ahn, Jae Hyuk Lee, Jaeku Park, Intae Eom, Minseok Kim, Sae Hwan Chun, Joonghan Kim, Hyotcherl Ihee,* and Jeongho Kim*



ARTICLE

https://doi.org/10.1038/s41467-021-25070-z OPEN

Filming ultrafast roaming-mediated isomerization of bismuth triiodide in solution

Eun Hyuk Choi^{1,2}, Jong Goo Kim^{1,2}, Jungmin Kim^{1,2}, Hosung Ki^{1,2}, Yunbeom Lee^{1,2}, Seonggon Lee^{1,2}, Kihwan Yoon³, Joonghan Kim³, Jeongho Kim⁴ & Hyotcherl Ihee^{1,2,23}

Ultrafast Carrier–Lattice Interactions and Interlayer Modulations of Bi₂Se₃ by X-ray Free-Electron Laser Diffraction

Sungwon Kim, Youngsam Kim, Jaeseung Kim, Sungwook Choi, Kyuseok Yun, Dongjin Kim, Soo Yeon Lim, Sunam Kim, Sae Hwan Chun, Jaeku Park, Intae Eom, Kyung Sook Kim, Tae-Yeong Koo, Yunbo Ou, Ferhat Katmis, Haidan Wen, Anthony DiChiara, Donald A. Walko, Eric C. Landahl, Hyeonsik Cheong, Eunji Sim, Jagadeesh Moodera, and Hyunjung Kim*

PHYSICAL REVIEW LETTERS 127, 175003 (2021)

Investigation of Nonequilibrium Electronic Dynamics of Warm Dense Copper with Femtosecond X-Ray Absorption Spectroscopy

Jong-Won Lee^{1,2,†,*} Minju Kim^{1,2,†} Gyeongbo Kang,^{1,2} Sam M. Vinko,^{3,4} Leejin Bae,⁵ Min Sang Cho^{1,2} Hyun-Kyung Chung,⁶ Minseok Kim,⁷ Soonnam Kwon,⁷ Gysang Lee,^{1,2} Chang Hee Nam,^{1,2} Sang Han Park^{1,7} Jang Hyeob Sohn,² Seong Hyeok Yang,² Ulf Zastrau,⁸ and Byoung Ick Cho^{1,2,*}

Ligand-Field Effects in a Ruthenium(II) Polypyridyl Complex Probed by Femtosecond X-ray Absorption Spectroscopy

Yujin Kim,[⊥] Rory Ma,[⊥] Junho Lee,[⊥] Jessica Harich, Daewoong Nam, Sangsoo Kim, Minseok Kim, Miguel Ochmann, Intae Eom, Nils Huse,* Jae Hyuk Lee,* and Tae Kyu Kim*

PHYSICAL REVIEW X 12, 011013 (2022)

Ultrafast Renormalization of the On-Site Coulomb Repulsion in a Cuprate Superconductor

Denitsa R. Baykusheva^{1,*} Hoyoung Jang² Ali A. Husain^{3,4,5} Sangjun Lee^{3,4} Sophia F. R. TenHuisen^{1,6} Preston Zhou,¹ Sunwook Park,^{7,8} Hoon Kim,^{7,8} Jin-Kwang Kim^{7,8} Hyeong-Do Kim² Minseok Kim,² Sang-Youn Park² Peter Abbamonte^{3,4} B. J. Kim,^{7,8} G. D. Gu,⁹ Yao Wang^{10,†} and Matteo Mitrano^{1,‡}

PLS-II

Energy upgrade: 2.5 => 3.0 GeV

Top-up operation

Normal conducting RF => Super conducting RF

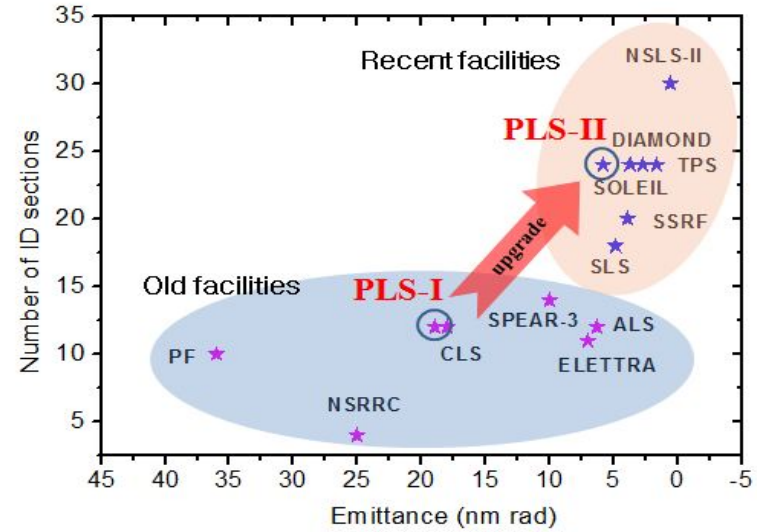
One year for user beam-time interruption

PLS-II Upgrade Storage Ring

○ Main goals

- Beam energy : 2.5 → 3.0 GeV
- Current : 200 → 400 mA
- Storage Ring Emittance : 18.9 → 5.8 nm
- Top-up Operation mode
- No. of Insertion Device : 10 → 20
- Superconducting RF cavities

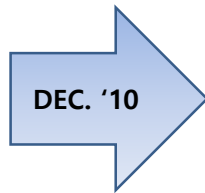
The 3rd generation synchrotron facilities



PLS



Dismantling



DEC. '10



Re-installation



JAN. '11



PLS-II

PLS



PLS-II



PLS-II Linac



Gallery

- Thermionic Electron Gun
- 17 Pulse Modulators (200MW, 7.5 μ s)
- 17 Klystrons (80 MW, 4 μ s)
- 16 Energy Doublers (gain=1.5)
- 46 Accelerating Sections

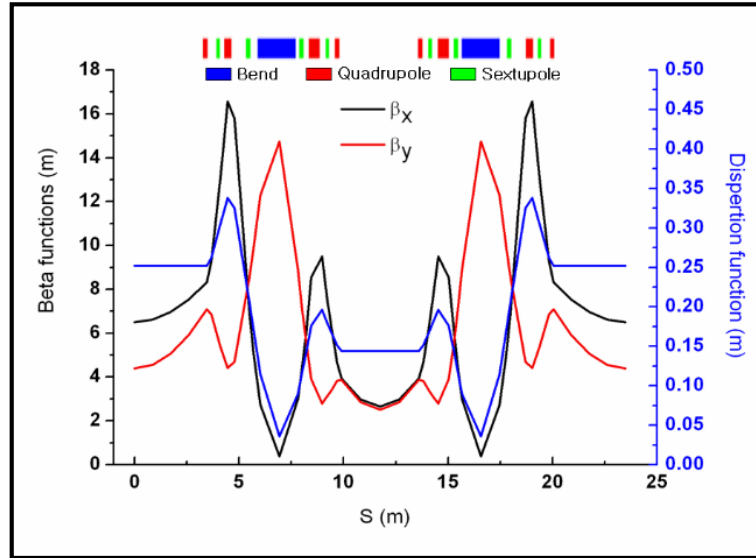
Injector LINAC

- Length = 170m
- 3.0 GeV, full energy injection
- 2,856 MHz (S-band)
- 10 Hz, 1.5 ns, 1 \AA pulsed beam
- Norm. emittance: 150 μ rad

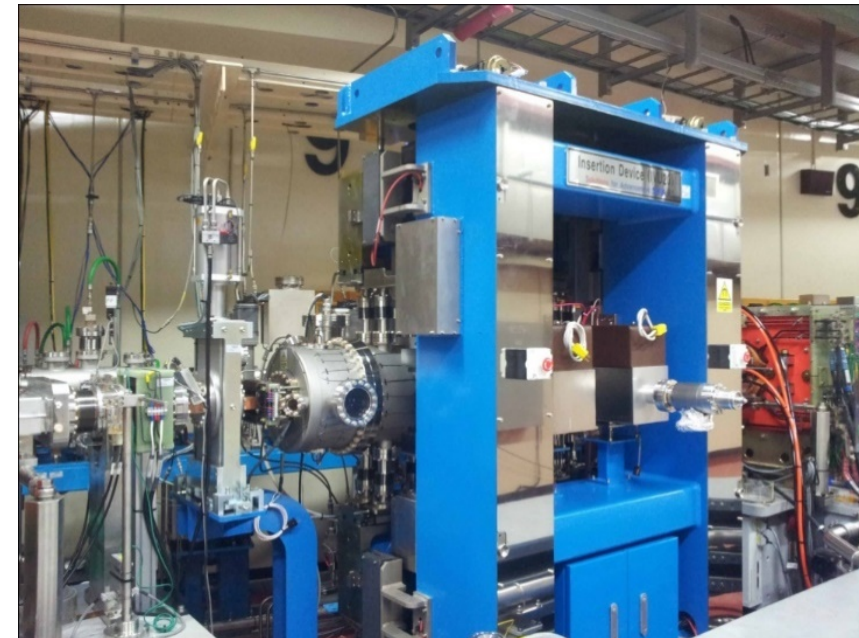


Tunnel

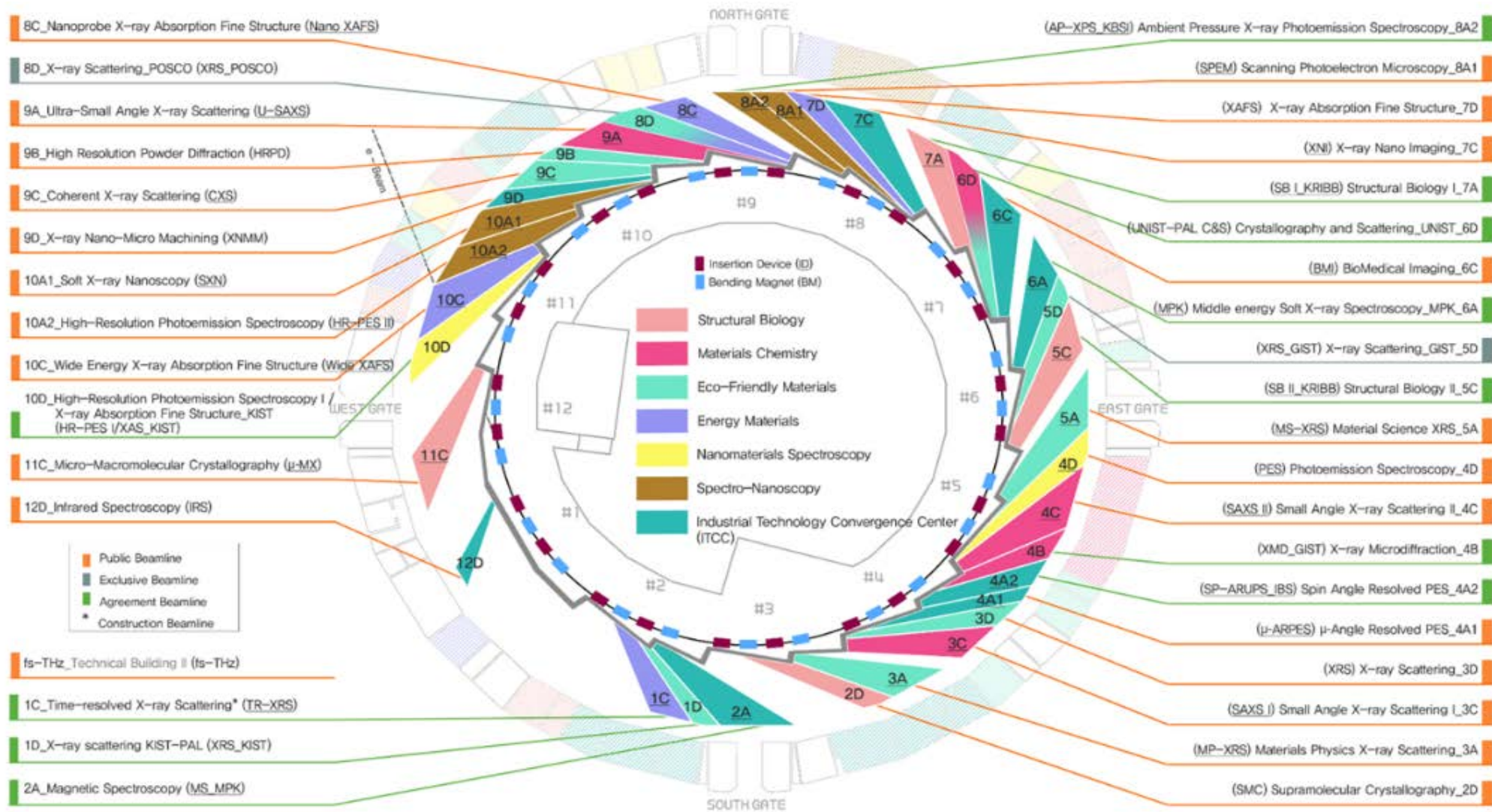
PLS-II Parameters



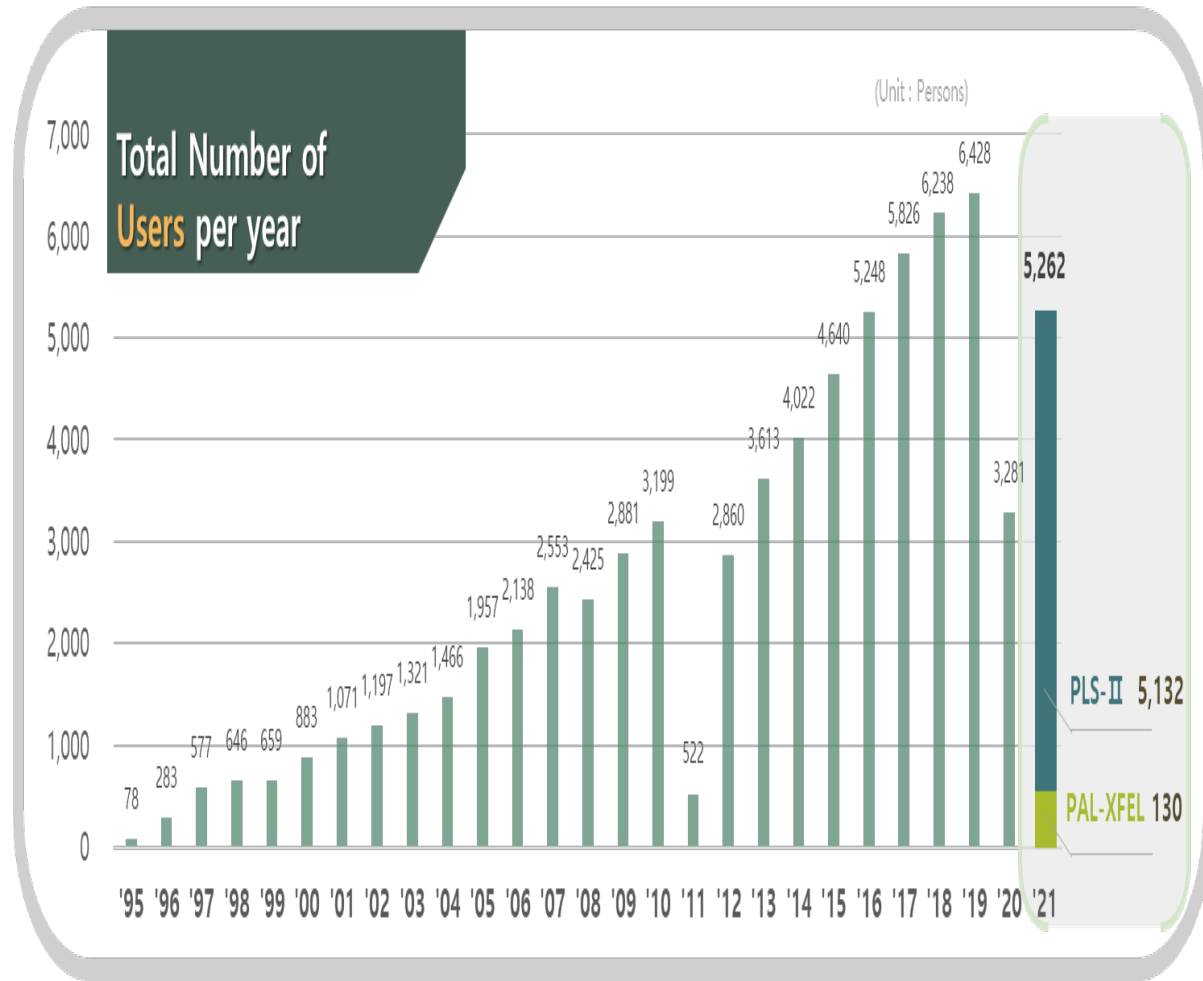
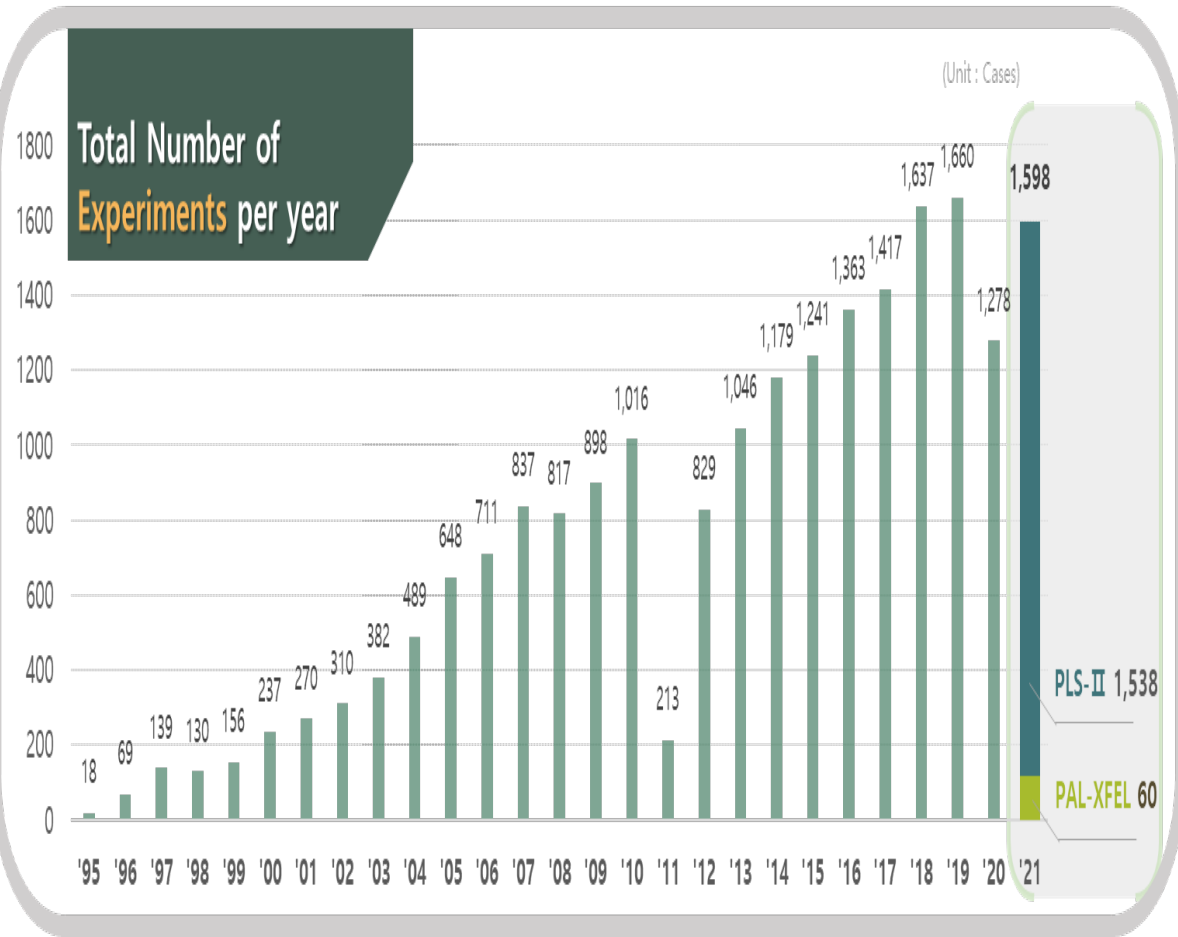
- **Beam Energy** 3.0 GeV
- **Beam Current** 400 mA
- **Lattice** DBA
- **Superperiods** 12
- **Emittance** 5.8 nm·rad
- **Tune** 15.37 / 9.15
- **SRF Frequency** 499.97 MHz
- **Circumference** 280 m



36 Beam-lines at PLS-II

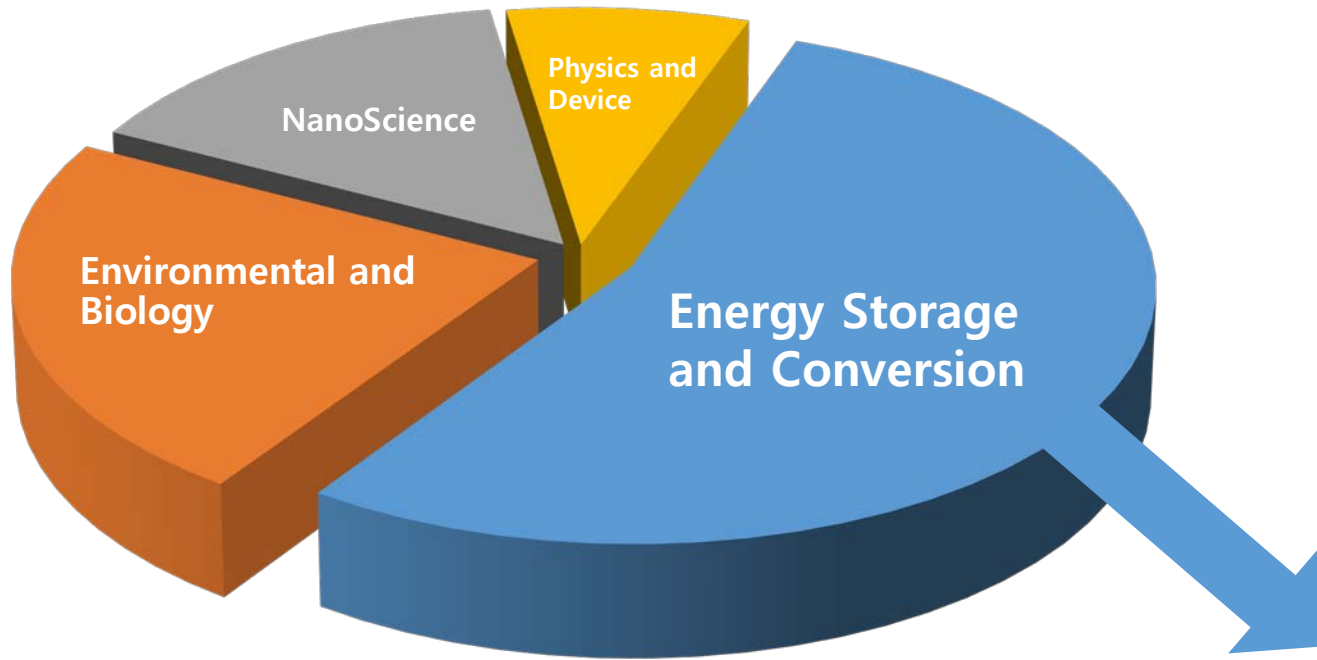


Number of Experiments and Users per Year

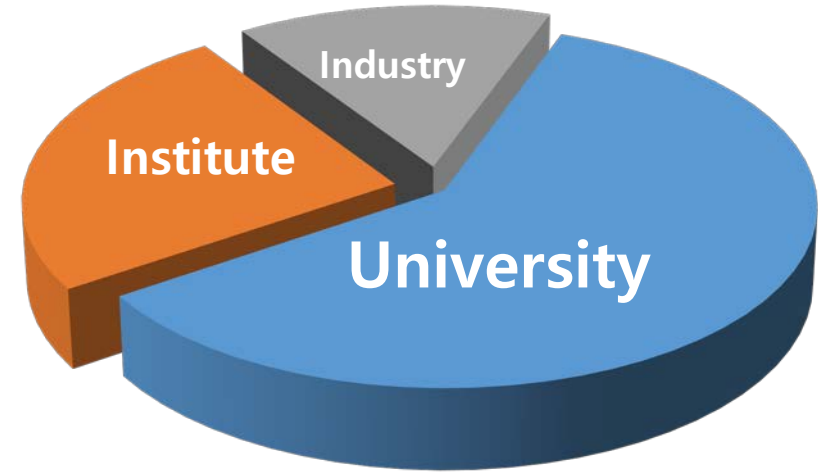


User Sciences in PLS-II

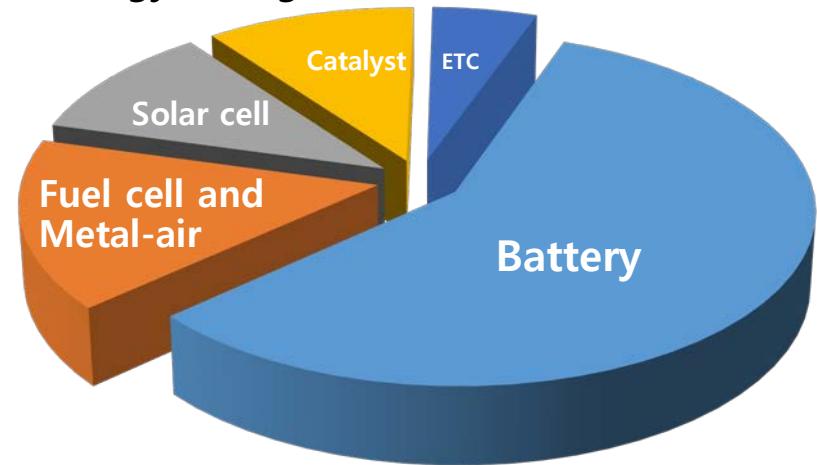
Research Fields



User Affiliations



Energy Storage and Conversion



- Blue** Li-ion battery*, Fuel cell, Solar cell and Metal-Air battery, Photocatalyst
- Orange** Drug design, Environmental materials, Biomass, Micro-organics
- Grey** Nanochemistry & Engineering
- Yellow** Memory*, Semiconductor, Display

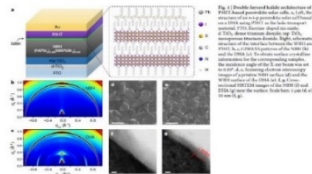
2020-2021 User Scientific Representative Achievements-I

Focused on Energy conversion and storage Materials and Nanochemistry

nature LETTER

Efficient, stable and scalable perovskite solar cells using poly(3-hexylthiophene)

Perovskite solar cells with high efficiency, stability and scalability are essential for the commercialization of perovskite solar cells. Here, we report a scalable and efficient perovskite solar cell using poly(3-hexylthiophene) (P3HT) as a hole-transporting material. The P3HT-based solar cell shows a power conversion efficiency of 22.1% under 1-sun illumination, which is comparable to that of the best-performing perovskite solar cells. The P3HT-based solar cell also shows excellent stability and scalability, with a power conversion efficiency of 20.1% after 1000 h of continuous illumination and a power conversion efficiency of 19.1% after 1000 h of continuous illumination under 1-sun illumination. The P3HT-based solar cell is also scalable, with a power conversion efficiency of 19.1% for a 1-cm² device.



Solar cell



Electrocatalyst

ARTICLES

Atomic-level tuning of Co-N-C catalyst for high-performance electrochemical H₂O₂ production

Euiyeon Jung^{1,2*}, Heejong Shin^{1,2*}, Byoung-Hoon Lee^{1,2}, Vladimir Efremov¹, Suhyeong Lee¹, Hyeon Seok Lee¹, Jihoon Kim¹, Wytse Hoeh Antink¹, Subin Park¹, Kug-Seung Lee¹, Sung-Pyo Cho¹, Jong Suk Yoo^{1,2}, Yung-Eun Sung^{1,2} & Taegwan Hyun^{1,2}

Despite the growing demand for hydrogen peroxide it is almost exclusively manufactured by the energy-intensive anthraquinone process. Alternatively, H₂O₂ can be produced electrochemically via the two-electron oxygen reduction reaction, although the performance of the state-of-the-art electrocatalysts is insufficient to meet the demands for industrialization. Interestingly, guided by first-principles calculations, we found that the catalytic properties of the Co-N_x moiety can be tailored by fine-tuning its surrounding atomic configuration to reproduce the structure-dependent catalytic properties of metalloenzymes. Using this principle, we designed and synthesized a single-atom electrocatalyst that comprises an optimized Co-N_x moiety incorporated in nitrogen-doped graphene for H₂O₂ production and exhibits a kinetic current density of 2.3 mA cm⁻² at 0.63 V versus the reversible hydrogen electrode and a mass activity of 0.85 A g⁻¹ at 0.65 V versus the reversible hydrogen electrode with negligible activity loss over 100 h.

Hydrogen peroxide (H₂O₂) is one of the most important chemicals as it plays a crucial role in the chemical and medical industries¹. The industrial production of H₂O₂ is heavily dependent on the anthraquinone process, which is an energy-intensive process that involves the hydrogenation of 2,2,6,6-tetramethylpiperidine using expensive palladium catalyst². Therefore, an electrochemical H₂O₂ production under ambient conditions is highly desirable. The electrocatalytic production of H₂O₂ by noble metal-based electrocatalysts (such as Au, Pt, Pd, Ir, Pt-Ir, Pt-C, and so on) has been shown to be effective^{3–5}. The surface electronic structure of noble metal

platforms for analyzing the cooperative interactions between metal centers and the surrounding atomic configurations^{6–9}. We are particularly interested in the N_x (N₂, N₃, N₄, transition metal) LCAO supported on graphene for two reasons. First, they can be regarded as metal centers surrounded by graphene-like ligands, similar to metalloenzymes, and second, N_x-N_x LCAOs can be highly active for a variety of electrocatalytic reactions^{10–12}. Although Pt, Ni, and Cu have proved to be highly active for the oxygen reduction reaction (ORR) (mainly for four electron ORR) in aqueous media, the general principle that governs their selectivity towards H₂O₂ has not been elucidated¹³.

Li-ion Battery

NATURE MATERIALS | VOL. 19 | APRIL 2020 | 419–427 | www.nature.com/naturematerials



Voltage decay and redox asymmetry mitigation by reversible cation migration in lithium-rich layered oxide electrodes

Donggan Eum¹, Byunghoon Kim^{1,2}, Sang Joo Kim¹, Hyeonjun Park¹, Jinsung Wu^{1,2}, Sang-Pyo Cho¹, Gabin Yoon¹, Myoung Hwan Lee¹, Sung-Kyun Jung^{1,2}, Wanli Yang¹, Won Mo Seong¹, Kyujin Ku¹, Orapa Tamwatantana¹, Sung Kwan Park¹, Insang Hwang¹ & Kisuk Kang^{1,2*}

Despite the high energy density of lithium-rich layered-oxide electrodes, their real-world implementation in batteries is hindered by the substantial voltage decay on cycling. This voltage decay is widely accepted to mainly originate from progressive structural rearrangements involving irreversible transition-metal migration. As prevention of this spontaneous cation migration has proved difficult, a paradigm shift toward management of its reversibility is needed. Here, we demonstrate that the reversibility of the cation migration of lithium-rich nickel manganese oxides can be remarkably improved by altering the oxygen stacking sequences in the layered structure and thereby drastically reducing the voltage decay. The prevented lithium-ion reversibility of the cation migration is experimentally visualized, and first-principles calculations reveal that an O2-type structure restricts the movements of transition metals within the Li layer, which effectively streamlines the returning migration path of the transition metals. Furthermore, we propose that the enhanced reversibility mitigates the asymmetry of the anionic redox in conventional lithium-rich electrodes, promoting the high-potential anionic redox, thereby reducing the subsequent voltage hysteresis. Our findings demonstrate that regulating the reversibility of the cation migration is a practical strategy to reduce voltage decay and hysteresis in lithium-rich layered materials.

With the advent of electric transportation, there is a growing demand for improvements in rechargeable lithium-ion batteries. In particular, the energy density stored on the cathode materials has been a primary factor

lithium-rich layered oxide^{1–3}. Cation migration from the transition and O2 layer to the Li layer to form O₂ and O₁ sites (cation-vacancy defect pair) during the charging of lithium-rich layered Ni metal oxides has been identified experimentally and on



Stabilization of formamidinium lead triiodide α -phase with isopropylammonium chloride for perovskite solar cells

Byung-wook Park^{1,2}, Hyung Woo Kwon^{1,2}, Yonghui Lee¹, Do Yoon Lee¹, Min Gyu Kim^{1,2}, Geonhwa Kim^{1,2}, Ki-seong Kim¹, Young Ki Kim¹, Jimo Im^{1,2}, Tae Joo Shin^{1,2} & Sang Il Seok^{1,2}

Formamidinium lead triiodide (FAPbI₃) perovskite solar cells (PSCs) are mainly fabricated by sequentially coating lead iodide and formamidinium iodide, or by coating a solution in which all components are dissolved (one-pot process). The PSCs produced by both processes exhibited similar efficiencies; however, their long-term stabilities were notably different. We concluded that the major reason for this behavior is the stabilization of the α -FAPbI₃ phase by isopropylammonium cations produced by the chemical reaction between isopropyl alcohol, used as a solvent, and methylammonium chloride, added during the process. On this basis, we fabricated PSCs by adding isopropylammonium chloride to the perovskite precursor solution for the one-pot process and achieved a certified power conversion efficiency of 23.9%. Long-term operational current density-voltage measurements (one sweep every 84 min under 1-sun irradiation in nitrogen atmosphere) showed that the as-fabricated device with an initial efficiency of approximately 20% recorded an efficiency of about 23% after 1,000 h that gradually degraded to about 22% after an additional 1,000 h.

nature Nanochemistry

ARTICLES

Design and synthesis of multigrain nanocrystals via geometric misfit strain

Received 15 June 2019
Revised 20 October 2019
Accepted 20 October 2019
Published online 15 January 2020

Myoung Hwan Cho^{1,2,3,4,5,6,7,8,9,10,11,12,13,14,15,16,17,18,19,20,21,22,23,24,25,26,27,28,29,30,31,32,33,34,35,36,37,38,39,40,41,42,43,44,45,46,47,48,49,50,51,52,53,54,55,56,57,58,59,60,61,62,63,64,65,66,67,68,69,70,71,72,73,74,75,76,77,78,79,80,81,82,83,84,85,86,87,88,89,90,91,92,93,94,95,96,97,98,99,100,101,102,103,104,105,106,107,108,109,110,111,112,113,114,115,116,117,118,119,120,121,122,123,124,125,126,127,128,129,130,131,132,133,134,135,136,137,138,139,140,141,142,143,144,145,146,147,148,149,150,151,152,153,154,155,156,157,158,159,160,161,162,163,164,165,166,167,168,169,170,171,172,173,174,175,176,177,178,179,180,181,182,183,184,185,186,187,188,189,190,191,192,193,194,195,196,197,198,199,200,201,202,203,204,205,206,207,208,209,210,211,212,213,214,215,216,217,218,219,220,221,222,223,224,225,226,227,228,229,230,231,232,233,234,235,236,237,238,239,240,241,242,243,244,245,246,247,248,249,250,251,252,253,254,255,256,257,258,259,260,261,262,263,264,265,266,267,268,269,270,271,272,273,274,275,276,277,278,279,280,281,282,283,284,285,286,287,288,289,290,291,292,293,294,295,296,297,298,299,300,301,302,303,304,305,306,307,308,309,310,311,312,313,314,315,316,317,318,319,320,321,322,323,324,325,326,327,328,329,330,331,332,333,334,335,336,337,338,339,340,341,342,343,344,345,346,347,348,349,350,351,352,353,354,355,356,357,358,359,360,361,362,363,364,365,366,367,368,369,370,371,372,373,374,375,376,377,378,379,380,381,382,383,384,385,386,387,388,389,390,391,392,393,394,395,396,397,398,399,400,401,402,403,404,405,406,407,408,409,410,411,412,413,414,415,416,417,418,419,420,421,422,423,424,425,426,427,428,429,430,431,432,433,434,435,436,437,438,439,440,441,442,443,444,445,446,447,448,449,450,451,452,453,454,455,456,457,458,459,460,461,462,463,464,465,466,467,468,469,470,471,472,473,474,475,476,477,478,479,480,481,482,483,484,485,486,487,488,489,490,491,492,493,494,495,496,497,498,499,500,501,502,503,504,505,506,507,508,509,510,511,512,513,514,515,516,517,518,519,520,521,522,523,524,525,526,527,528,529,530,531,532,533,534,535,536,537,538,539,540,541,542,543,544,545,546,547,548,549,550,551,552,553,554,555,556,557,558,559,560,561,562,563,564,565,566,567,568,569,570,571,572,573,574,575,576,577,578,579,580,581,582,583,584,585,586,587,588,589,590,591,592,593,594,595,596,597,598,599,600,601,602,603,604,605,606,607,608,609,610,611,612,613,614,615,616,617,618,619,620,621,622,623,624,625,626,627,628,629,630,631,632,633,634,635,636,637,638,639,640,641,642,643,644,645,646,647,648,649,650,651,652,653,654,655,656,657,658,659,660,661,662,663,664,665,666,667,668,669,670,671,672,673,674,675,676,677,678,679,680,681,682,683,684,685,686,687,688,689,690,691,692,693,694,695,696,697,698,699,700,701,702,703,704,705,706,707,708,709,710,711,712,713,714,715,716,717,718,719,720,721,722,723,724,725,726,727,728,729,730,731,732,733,734,735,736,737,738,739,740,741,742,743,744,745,746,747,748,749,750,751,752,753,754,755,756,757,758,759,760,761,762,763,764,765,766,767,768,769,770,771,772,773,774,775,776,777,778,779,780,781,782,783,784,785,786,787,788,789,790,791,792,793,794,795,796,797,798,799,800,801,802,803,804,805,806,807,808,809,810,811,812,813,814,815,816,817,818,819,820,821,822,823,824,825,826,827,828,829,830,831,832,833,834,835,836,837,838,839,840,841,842,843,844,845,846,847,848,849,850,851,852,853,854,855,856,857,858,859,860,861,862,863,864,865,866,867,868,869,870,871,872,873,874,875,876,877,878,879,880,881,882,883,884,885,886,887,888,889,890,891,892,893,894,895,896,897,898,899,900,901,902,903,904,905,906,907,908,909,910,911,912,913,914,915,916,917,918,919,920,921,922,923,924,925,926,927,928,929,930,931,932,933,934,935,936,937,938,939,940,941,942,943,944,945,946,947,948,949,950,951,952,953,954,955,956,957,958,959,960,961,962,963,964,965,966,967,968,969,970,971,972,973,974,975,976,977,978,979,980,981,982,983,984,985,986,987,988,989,990,991,992,993,994,995,996,997,998,999,1000}

The impact of topological defects associated with grain boundaries (GB defects) on the electrical, optical, magnetic, mechanical and chemical properties of polycrystalline materials^{1–3} is well known. However, elucidating this influence experimentally is difficult because grains typically exhibit a large range of sizes, shapes and random relative orientations^{4–6}. Here we demonstrate that precise control of the heterogeneity of colloidal/polymorphic nanocrystals enables ordered grain growth and can thereby produce material samples with uniform GB defects. We illustrate our approach with a multigrain nanocrystal comprising Co₃O₄ nanocrystals that carries a Mn₂O₃ shell on each facet. The individual shells are symmetrically interconnected grains⁷, and the large geometric misfit between adjacent tetragonal Mn₂O₃ grains results in the boundaries at the sharp edges of the Co₃O₄ nanocrystals, not the joints via dislocations. We identify four design principles that govern the production of these highly ordered multigrain nanocrystals. First, the shape of the substrate nanocrystal must guide the crystallographic orientation of the overgrowth phase⁸. Second, the size of the substrate must be smaller than the characteristic distance between the dislocations. Third, the incompatible symmetry between the overgrowth phase and the substrate increases the geometric misfit strain between the grains. Fourth, for GB formation under near-equilibrium conditions, the surface energy of the shell needs to be balanced by the increasing elastic energy through ligand passivation⁹. With these principles, we can produce a range of multigrain nanocrystals containing distinct GB defects.

Memory device



A bioinspired and hierarchically structured shape-memory material

Luca Cera¹, Grant M. Gonzalez¹, Qihan Liu¹, Suji Choi¹, Christophe O. Chantre¹, Juncheol Lee^{1,2}, Rudy Gabardier¹, Myung Chul Cho¹, Kwamwo Shin¹ & Kevin Kit Parker^{1,2,3,4,5,6,7,8,9,10,11,12,13,14,15,16,17,18,19,20,21,22,23,24,25,26,27,28,29,30,31,32,33,34,35,36,37,38,39,40,41,42,43,44,45,46,47,48,49,50,51,52,53,54,55,56,57,58,59,60,61,62,63,64,65,66,67,68,69,70,71,72,73,74,75,76,77,78,79,80,81,82,83,84,85,86,87,88,89,90,91,92,93,94,95,96,97,98,99,100,101,102,103,104,105,106,107,108,109,110,111,112,113,114,115,116,117,118,119,120,121,122,123,124,125,126,127,128,129,130,131,132,133,134,135,136,137,138,139,140,141,142,143,144,145,146,147,148,149,150,151,152,153,154,155,156,157,158,159,160,161,162,163,164,165,166,167,168,169,170,171,172,173,174,175,176,177,178,179,180,181,182,183,184,185,186,187,188,189,190,191,192,193,194,195,196,197,198,199,200,201,202,203,204,205,206,207,208,209,210,211,212,213,214,215,216,217,218,219,220,221,222,223,224,225,226,227,228,229,230,231,232,233,234,235,236,237,238,239,240,241,242,243,244,245,246,247,248,249,250,251,252,253,254,255,256,257,258,259,260,261,262,263,264,265,266,267,268,269,270,271,272,273,274,275,276,277,278,279,280,281,282,283,284,285,286,287,288,289,290,291,292,293,294,295,296,297,298,299,300,301,302,303,304,305,306,307,308,309,310,311,312,313,314,315,316,317,318,319,320,321,322,323,324,325,326,327,328,329,330,331,332,333,334,335,336,337,338,339,340,341,342,343,344,345,346,347,348,349,350,351,352,353,354,355,356,357,358,359,360,361,362,363,364,365,366,367,368,369,370,371,372,373,374,375,376,377,378,379,380,381,382,383,384,385,386,387,388,389,390,391,392,393,394,395,396,397,398,399,400,401,402,403,404,405,406,407,408,409,410,411,412,413,414,415,416,417,418,419,420,421,422,423,424,425,426,427,428,429,430,431,432,433,434,435,436,437,438,439,440,441,442,443,444,445,446,447,448,449,450,451,452,453,454,455,456,457,458,459,460,461,462,463,464,465,466,467,468,469,470,471,472,473,474,475,476,477,478,479,480,481,482,483,484,485,486,487,488,489,490,491,492,493,494,495,496,497,498,499,500,501,502,503,504,505,506,507,508,509,510,511,512,513,514,515,516,517,518,519,520,521,522,523,524,525,526,527,528,529,530,531,532,533,534,535,536,537,538,539,540,541,542,543,544,545,546,547,548,549,550,551,552,553,554,555,556,557,558,559,560,561,562,563,564,565,566,567,568,569,570,571,572,573,574,575,576,577,578,579,580,581,582,583,584,585,586,587,588,589,590,591,592,593,594,595,596,597,598,599,600,601,602,603,604,605,606,607,608,609,610,611,612,613,614,615,616,617,618,619,620,621,622,623,624,625,626,627,628,629,630,631,632,633,634,635,636,637,638,639,640,641,642,643,644,645,646,647,648,649,650,651,652,653,654,655,656,657,658,659,660,661,662,663,664,665,666,667,668,669,670,671,672,673,674,675,676,677,678,679,680,681,682,683,684,685,686,687,688,689,690,691,692,693,694,695,696,697,698,699,700,701,702,703,704,705,706,707,708,709,710,711,712,713,714,715,716,717,718,719,720,721,722,723,724,725,726,727,728,729,730,731,732,733,734,735,736,737,738,739,740,741,742,743,744,745,746,747,748,749,750,751,752,753,754,755,756,757,758,759,760,761,762,763,764,765,766,767,768,769,770,771,772,773,774,775,776,777,778,779,780,781,782,783,784,785,786,787,788,789,790,791,792,793,794,795,796,797,798,799,800,801,802,803,804,805,806,807,808,809,810,811,812,813,814,815,816,817,818,819,820,821,822,823,824,825,826,827,828,829,830,831,832,833,834,835,836,837,838,839,840,841,842,843,844,845,846,847,848,849,850,851,852,853,854,855,856,857,858,859,860,861,862,863,864,865,866,867,868,869,870,871,872,873,874,875,876,877,878,879,880,881,882,883,884,885,886,887,888,889,890,891,892,893,894,895,896,897,898,899,900,901,902,903,904,905,906,907,908,909,910,911,912,913,914,915,916,917,918,919,920,921,922,923,924,925,926,927,928,929,930,931,932,933,934,935,936,937,938,939,940,941,942,943,944,945,946,947,948,949,950,951,952,953,954,955,956,957,958,959,960,961,962,963,964,965,966,967,968,969,970,971,972,973,974,975,976,977,978,979,980,981,982,983,984,985,986,987,988,989,990,991,992,993,994,995,996,997,998,999,1000}

Shape-memory polymeric materials lack long-range molecular order that enables more controlled and efficient actuation mechanisms. Here, we develop a hierarchical structured keratin-based system that has long-range molecular order and shape-memory properties in response to hydration. We explore the metastable configuration of the keratin secondary structure, the transition from α -helix to β -sheet, as an actuation mechanism to design a high-strength shape-memory material that is biocompatible and processible through fibre spinning and three-dimensional (3D) printing. We extract keratin protofibrils from animal hair and subject them to shear stress to induce their self-organization into a nematic phase, which recapitulates the native hierarchical organization of the protein. This self-assembly process can be tuned to create materials with desired anisotropic structuring and responsiveness. Our combination of bottom-up assembly and top-down manufacturing allows for the scalable fabrication of strong and hierarchically structured shape-memory fibres and 3D-printed scaffolds with potential applications in bioengineering and smart textiles.

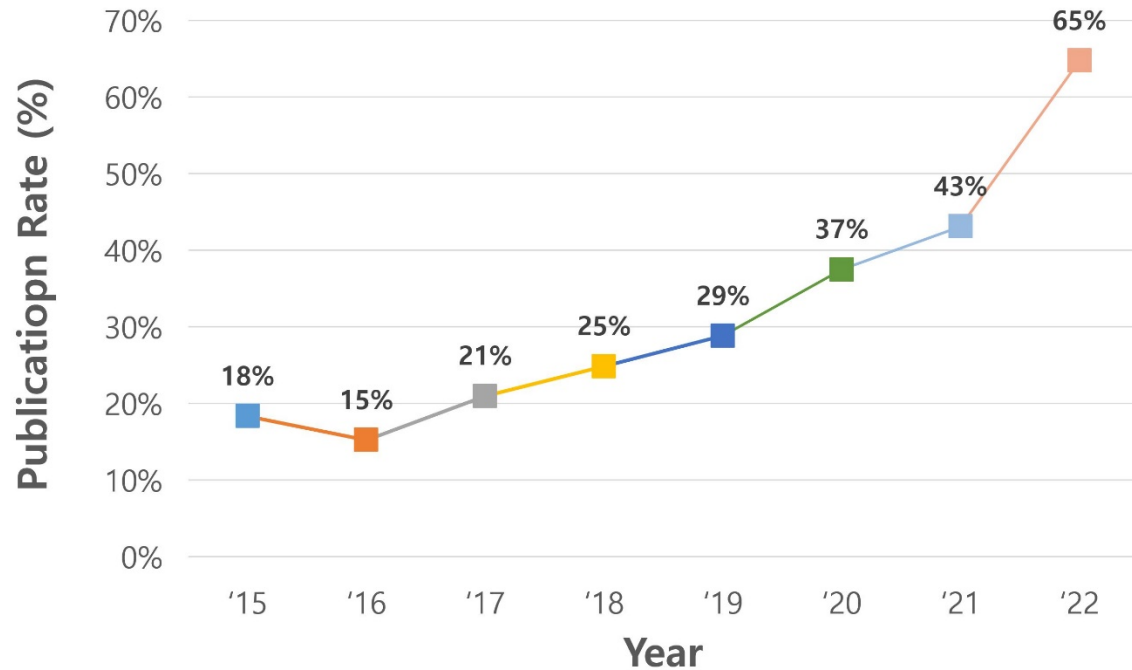
nature Catalyst

ARTICLES</

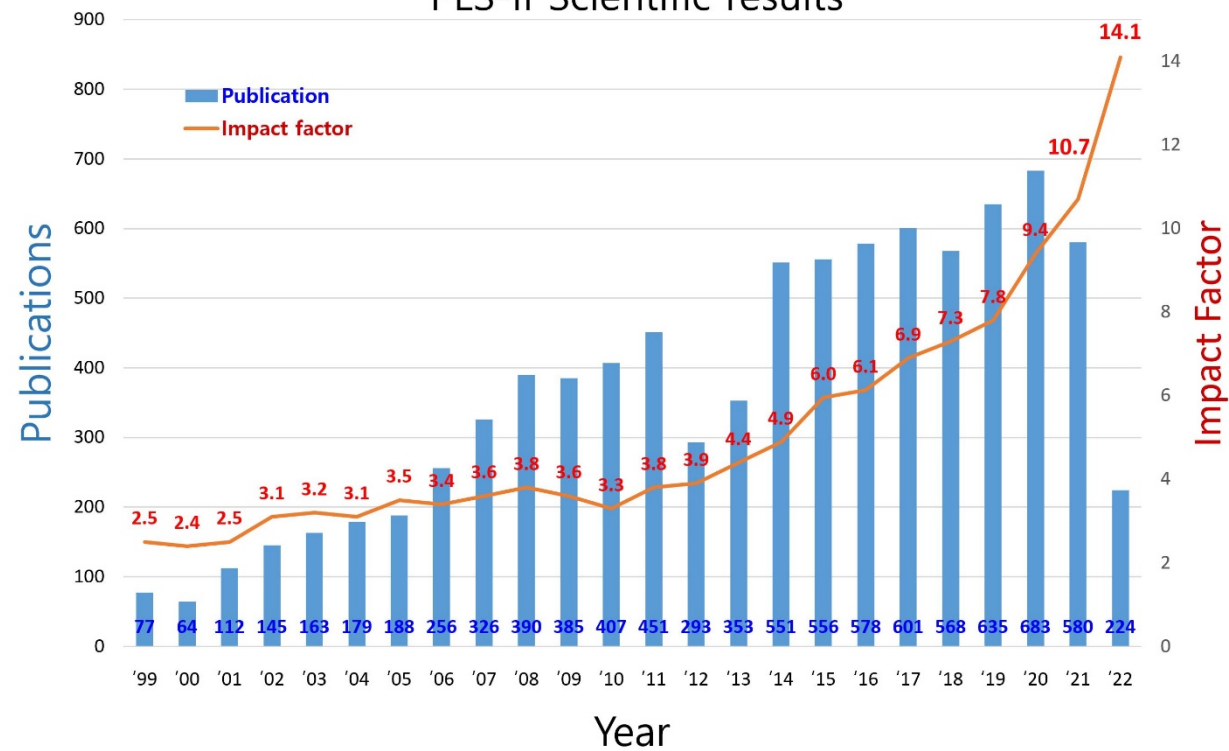
2022 User Scientific General Achievements-II

*An increasing trend of Impact factor
Constant SCI Publications*

Publication-Rate higher than Impact Factor 10



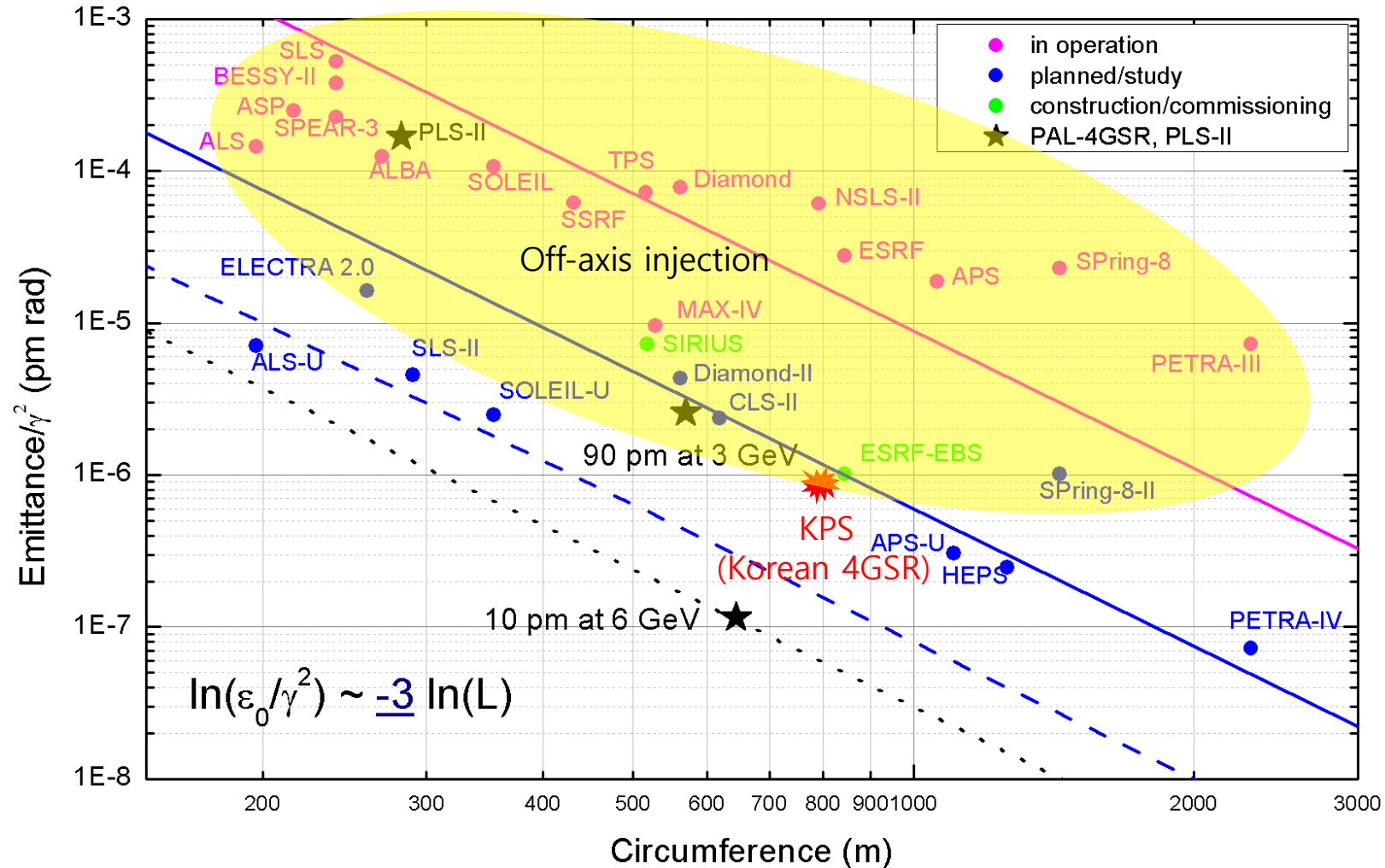
PLS-II Scientific results



KPS (Korea Photon Source)

Users are increasing
Available Beam-lines are limited at 36
High-performance beams are in demand
There is no space left at PAL

3rd and 4th Generation Light Sources

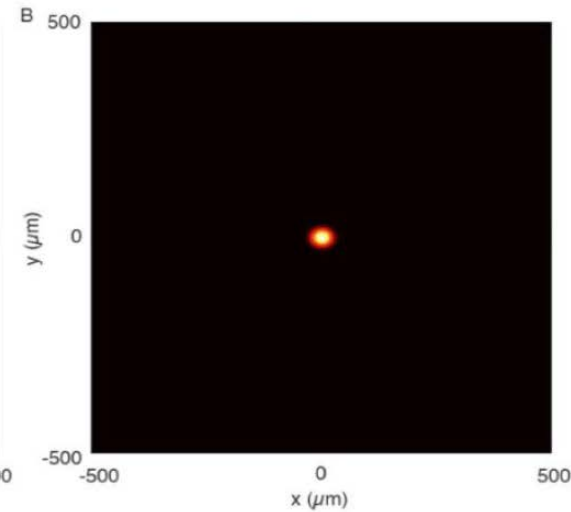
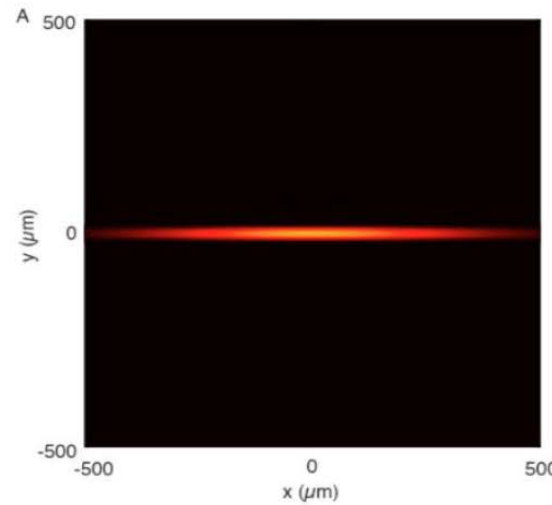
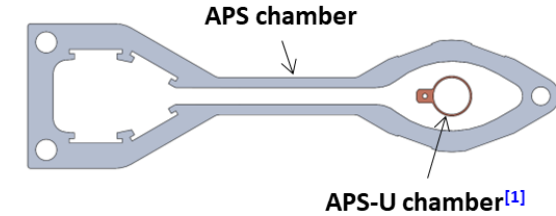
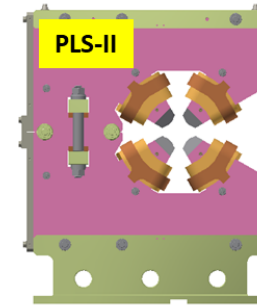
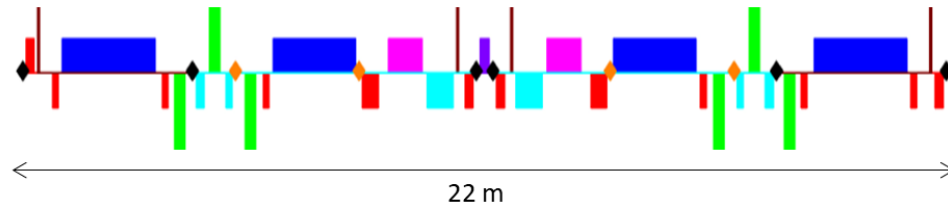


3GSR vs. 4GSR (with challenging technology)

- The 3rd Generation Storage Ring Lattice:



- The 4th Generation Storage Ring Lattice:



Korea Photon Source (KPS) Project

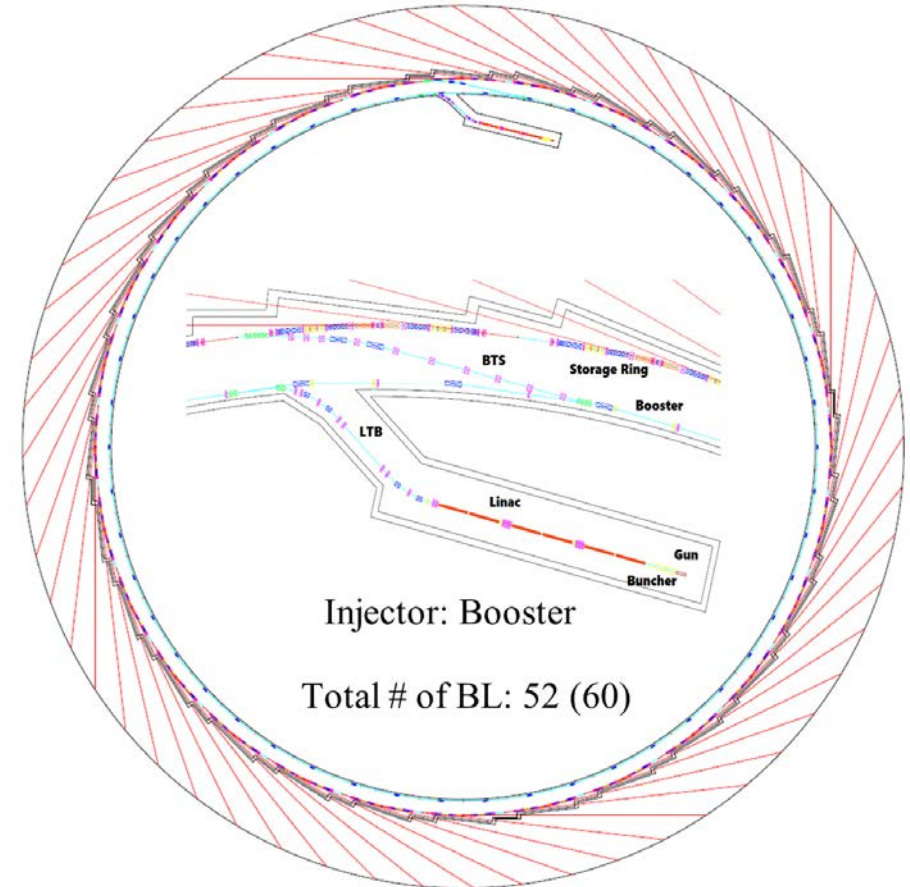
- Preliminary study by PAL: 2017 ~ 2019
- CDR project: 2020
- Project start: 2021. 7 ~ 2027. 12

 - Building by KBSI / Machine by PAL

Parameter	Units	PLS-II	Korean 4GSR
Electron energy	GeV	3	4
Horiz. Emittance	pm	5,800	58 (RB: 39)
Vert. Emittance	pm	~ 58	~ 5.8 (RB: 39)
Bunch length (rms)	ps	20	13 (50 with HC)
Circumference	m	280	800
Harmonic #		470	1332
RF frequency	MHz	500	500
Beam stability @ ID (x/y)	μm	< 4 / 2	< 2.5 / 0.45
Injection mode		Top-up	Top-up

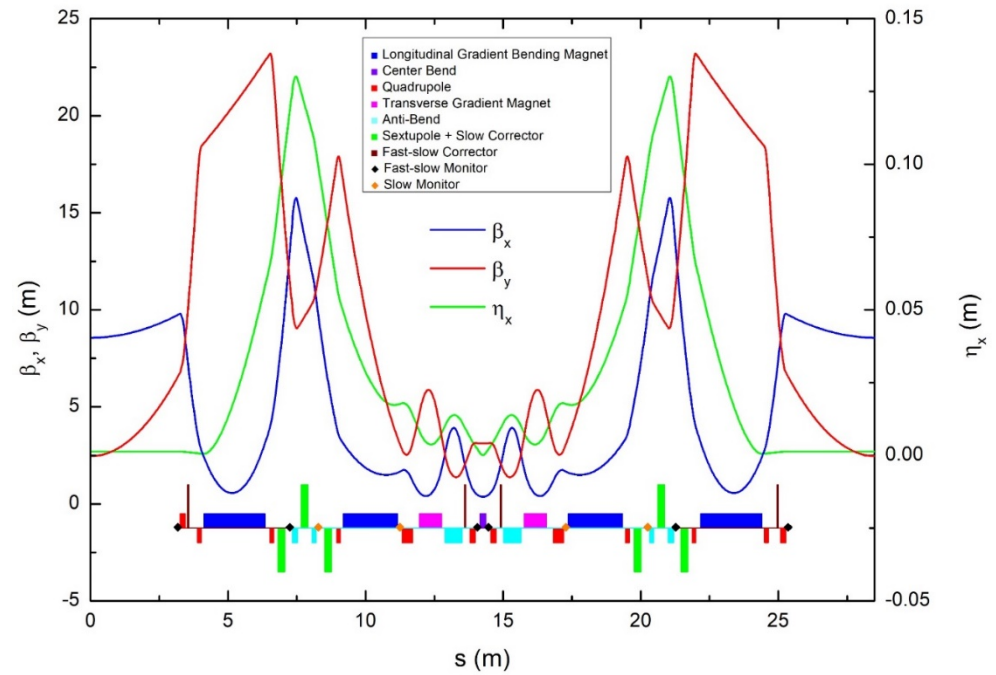
Major Parameters for KPS

4GSR Ring		Value	Unit
Design Parameters	Cell Number	28	-
	Circumference	798.84	[m]
	Electron Energy	4	[GeV]
	Natural Emittance	58	[pm rad]
Tune and Chromaticity	Horizontal Tune	67.395	-
	Vertical Tune	24.275	-
	Natural Horizontal Chromaticity	-115.344	-
	Natural Vertical Chromaticity	-84.693	-
	Horizontal Chromaticity	3.5	(target)
	Vertical Chromaticity	3.5	(target)
Radiation related quantities	Energy Loss per Turn	1009	[keV]
	Energy Spread	0.1197	[%]
	Horizontal Damping Time	11.075	[ms]
	Vertical Damping Time	21.127	[ms]
	Longitudinal Damping Time	19.342	[ms]
Twiss functions at the ID	Horizontal beta function at the ID center	8.564	[m]
	Vertical beta function at the ID center	2.459	[m]
	Dispersion function at the ID center	132	[mm]

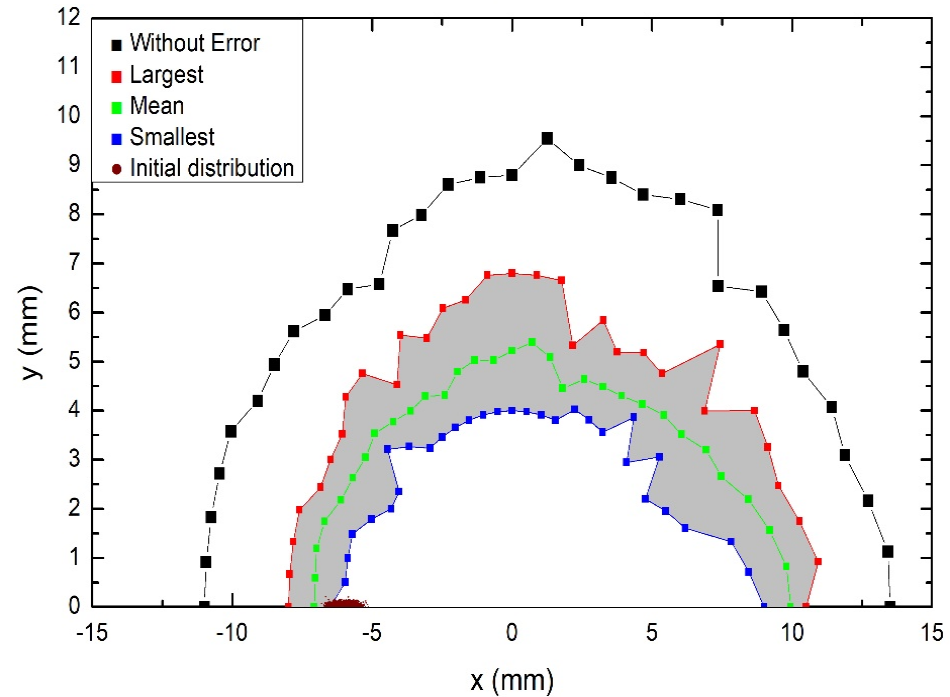
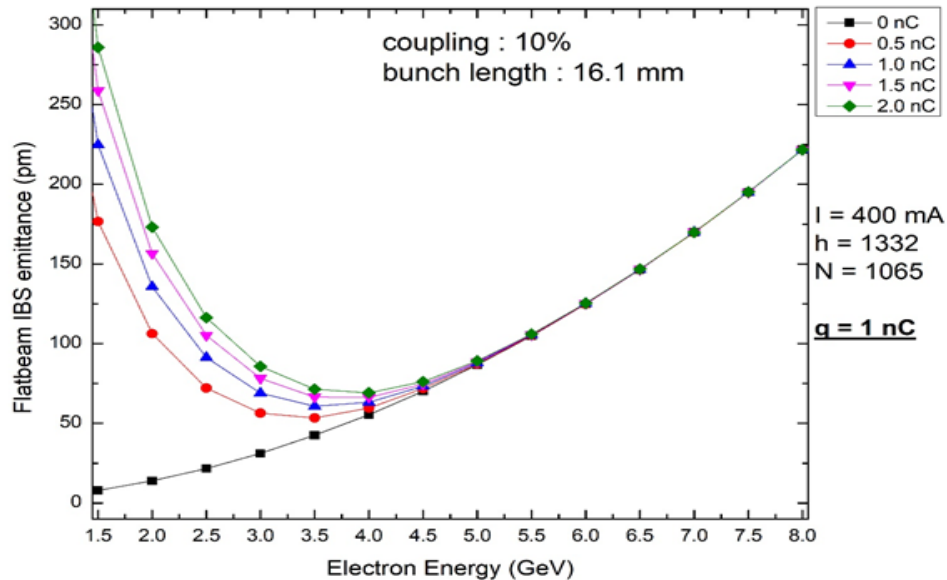


SR Lattice Structure (linear)

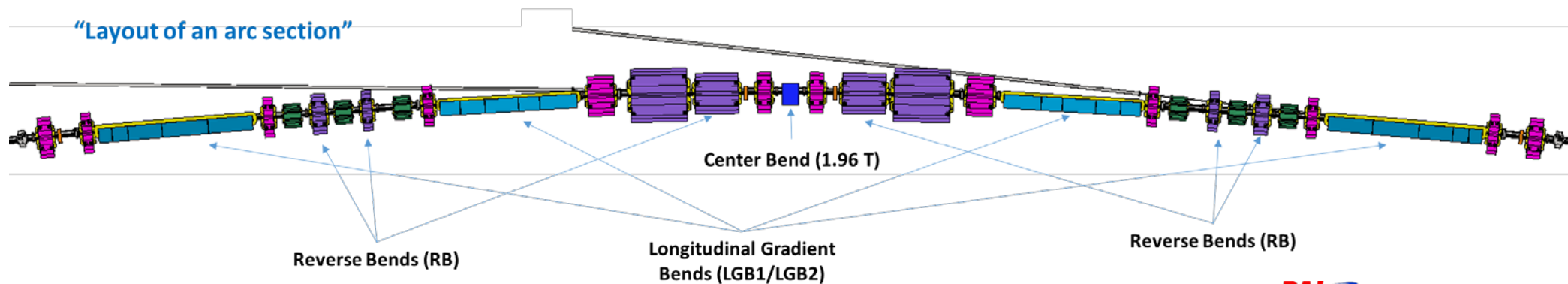
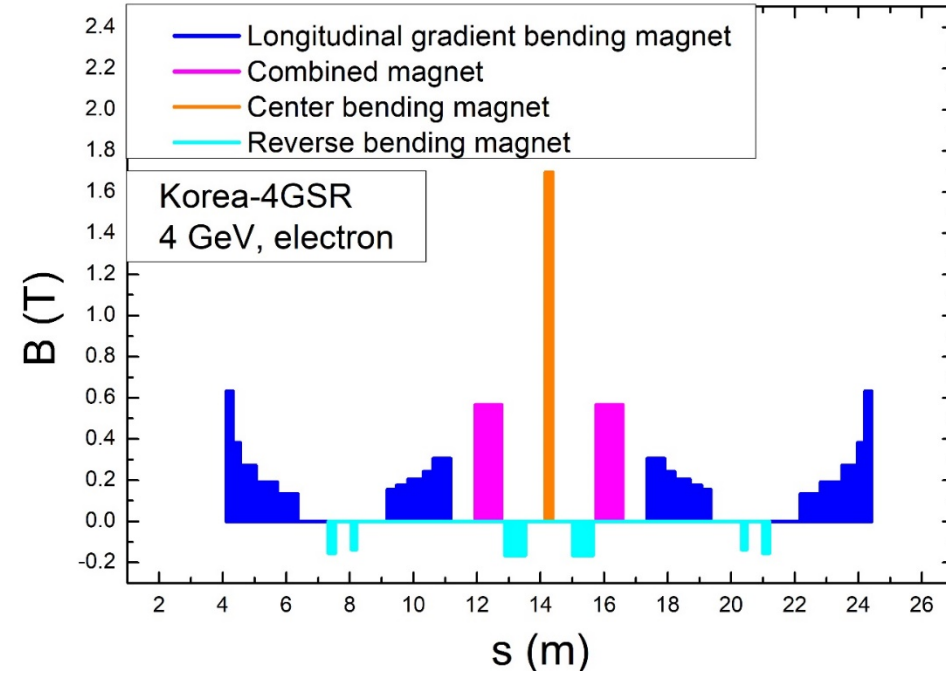
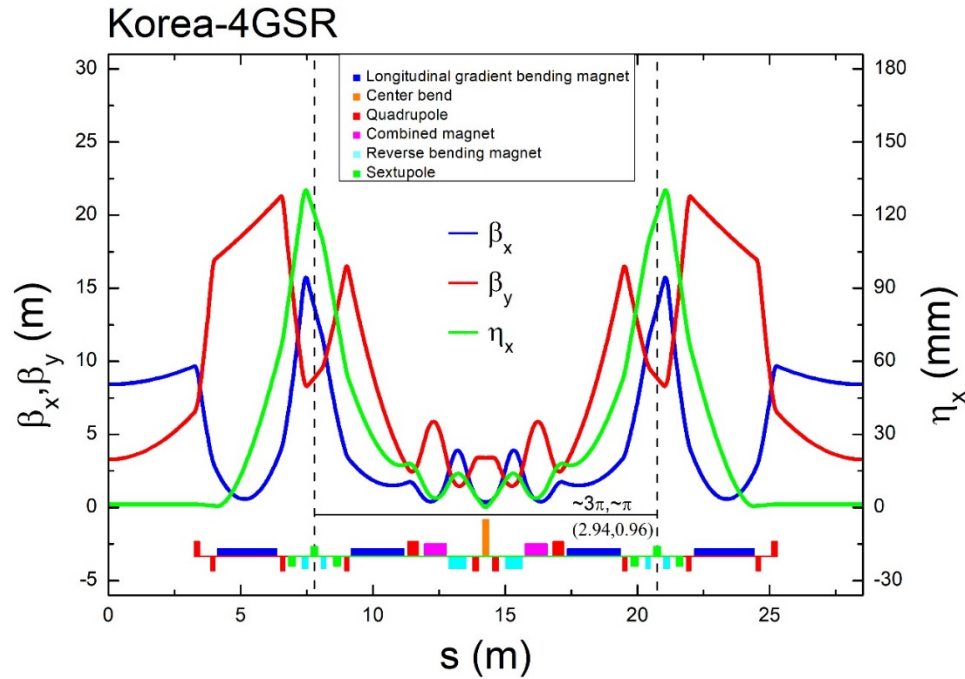
1. Natural evolution of ESRF-EBS and APS-U
2. ESRF-EBS type
 - Dispersion bump w/sextupoles.
 - Longitudinal gradient dipoles.
 - Phase advance of $\Delta\phi_x \sim 3\pi$ and $\Delta\phi_y \sim \pi$ between corresponding sextupole
3. APS-U type: Reverse bends in Q4, Q5, and Q8.
4. Massive use of combined function magnets
5. 6.5 m straight section and 2 T center-bend ($E_c=21$ keV)



Minimum emittance @ 4 GeV

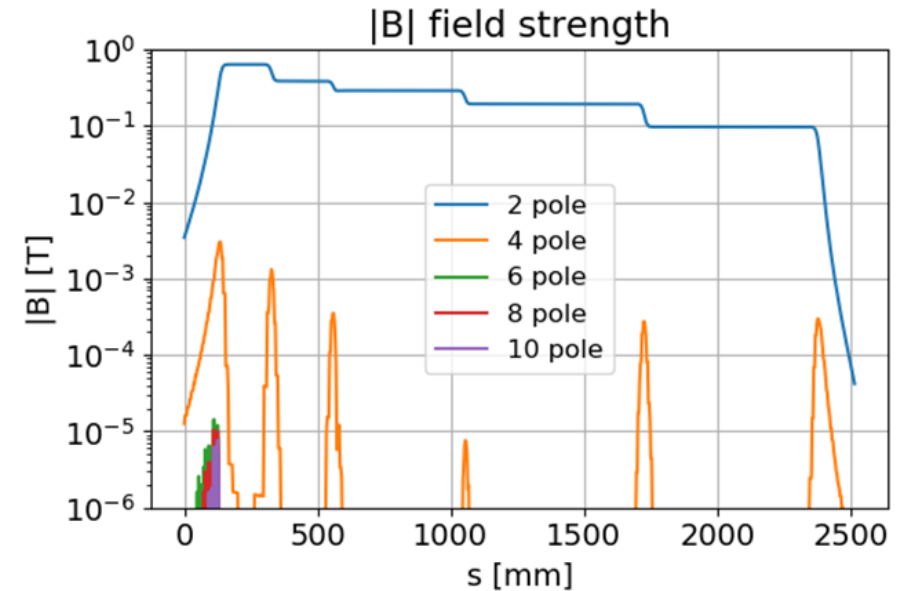
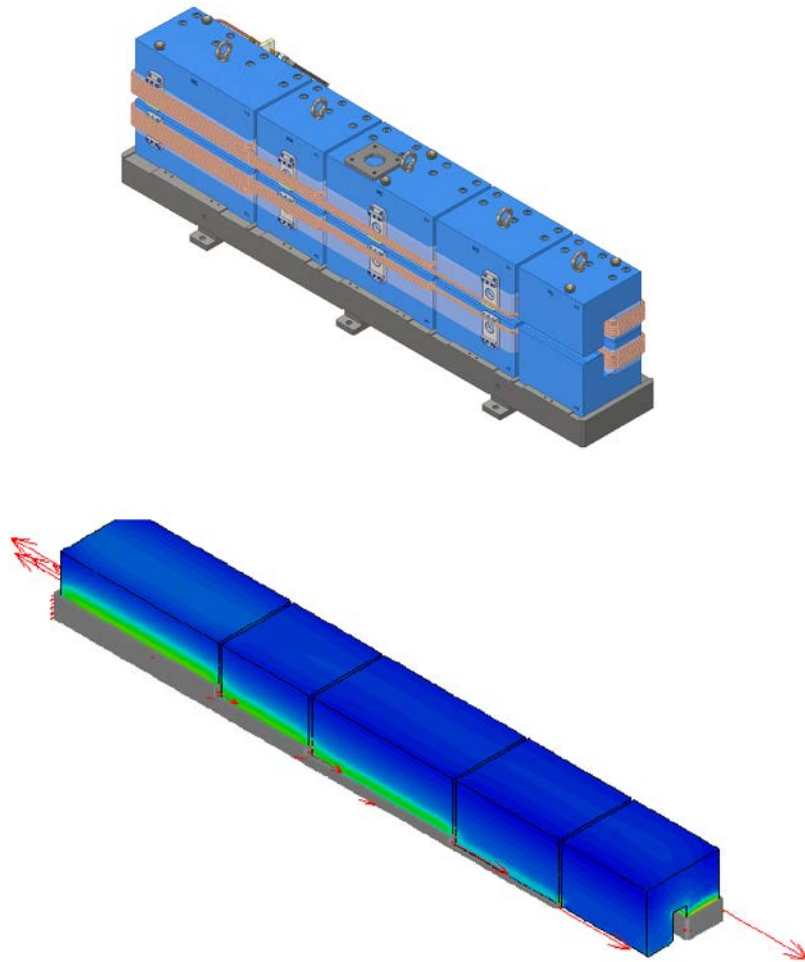


Hybrid 7-bend Achromat



Longitudinal Gradient Bending Magnet (LGBM)

Dipole and higher order multipole along the orbit.



- EM version is selected for construction costs and total cost of operation during the lifetime.
- 3D field map with 1mm step size is calculated, and the multipole along the orbit is calculated.
- Except the quadrupole component which comes from the edge focusing, higher order was negligible.
- To match the design field, reluctance gap at the return yoke is implemented for each magnet section.

Design Features

- ❖ **High photon beam performance from storage ring.**
 - **The best performance in the range of 10 ~ 40 keV.**
 - **Capability to generate photon beam up to 100 keV.**

- ❖ **Considering well demonstrated technologies for the design.**
 - **Off axis injection with conventional injection scheme**
 - **General technologies for magnet and vacuum systems.**

- ❖ **Synergy with PLS-II and PAL-XFEL.**
 - **Supporting full range of synchrotron radiation application.**

Initial Beam-lines (10 units)

Beam-line	Beam Energy	Resolution	Source	Experimental Technique
① BioPharma-BioSAXS	5~20 keV	SAXS: $< 1 \text{ \AA}$ $\Delta E/E < 10^{-4}$	IVU	① Bio-SAXS
② Material Structure Analysis	5~40 keV	$\Delta E/E < 10^{-4}$	Undulator	① XRD ② XAFS
③ Soft X-ray Nano-probe	0.1~5.0 keV	sub-micro beam $\Delta E/E > 1.5 \times 10^{-4} @ 1 \text{ keV}$	EPU	① XAS ② XPS
④ Nanoscale Angle-resolved Photoemission	0.1~2 keV	$< 100 \text{ nm}$ $\Delta E/E < 10^{-4}$	Undulator	① Nano-ARPES
⑤ Coherent X-ray Diffraction	3~30 keV	sub-micro beam	Undulator	① XRD ② CDI
⑥ Coherent Small-angle X-ray Scattering	4~40 keV	few nm ~ few μm $\Delta E/E < 2 \times 10^{-4}$	IVU	① SAXS/WAXS ② XPCS
⑦ Real-time X-ray Absorption Fine Structure	5~40 keV	Few μm	Undulator	① XAFS
⑧ Bio Nano crystallography	5~20 keV	$< 1 \text{ \AA}$	IVU	① MX
⑨ High Energy Microscopy	5 ~ 100 keV	resolution 0.1 μm	Superbend	① Projection imaging
⑩ Nano-probe	5~25 keV	$< 50 \text{ nm}$ 1~10 μm	IVU	① Ptychography/XRF ② XRS

Site Arrangement (Plan)



Summary

- **A few visionary people initiated light source facility in Korea in late 1980s.**
- **Successful constructions and user services at PAL have been recognized**
- **There are more accelerator projects being undertaken recently.**
- **The users' quality is continuously improved, and we expect more impact results.**
- **We need more technological development for effective domestic maintenance capability, for example, high-power klystrons, superconducting cavities, and cryogenic facilities.**

Acknowledgements

Thanks to

C. B. Kim: PAL-XFEL

I. T. Uom: PAL-XFEL

S. H. Shin: PLS-II

M. K. Kim: PLS-II

K. W. Kim: PAL

I. S. Ko: KPS

for their contribution



First Publication by First User



Draft Manuscript: Confidential

18 August 2017

Title: Maxima in the Thermodynamic Response and Correlation Functions of Deeply Supercooled Water

Authors: Kyung Hwan Kim^{1†}, Alexander Späh^{1†}, Harshad Pathak¹, Fivos Perakis¹, Daniel Mariedahl¹, Katrin Amann-Winkel¹, Jonas A. Sellberg², Jae Hyuk Lee³, Sangsoo Kim³, Jaehyun Park³, KiHyun Nam³, Tetsuo Katayama⁴, and Anders Nilsson^{1,*}

Affiliations:

¹Department of Physics, AlbaNova University Center, Stockholm University, SE-10691 Stockholm, Sweden

²Biomedical and X-Ray Physics, Department of Applied Physics, AlbaNova University Center, KTH Royal Institute of Technology, SE-10691 Stockholm, Sweden

³Pohang Accelerator Laboratory, Pohang, Gyeongbuk 37673, Republic of Korea

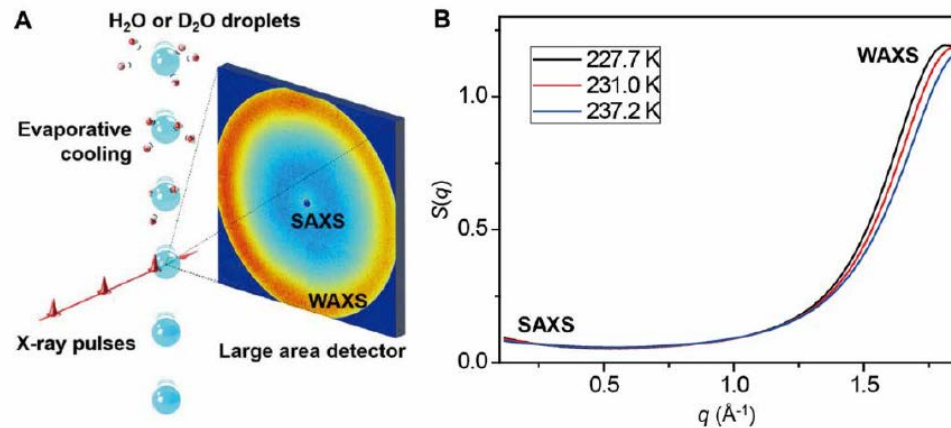
⁴Japan Synchrotron Radiation Research Institute, Kouto 1-1-1, Sayo, Hyogo 679-5198, Japan

*Corresponding author. E-mail: andersn@fysik.su.se

[†]These authors equally contributed to this work.

Abstract:

Femtosecond x-ray laser pulses were used to probe micron-sized water droplets cooled down to 227 K. From the x-ray scattering at the low momentum transfer region the isothermal compressibility and correlation length were extracted and the temperature dependence shows maxima at 229 K for H₂O and 233 K for D₂O. In addition, from the first diffraction peak it was observed that the liquid undergoes the most rapid growth of tetrahedral structures at similar temperatures. These observations point to the existence of a Widom line, defined as the locus of maximum correlation length emanating from a critical point at positive pressures deeply in the supercooled regime. The difference in maximum value of the isothermal compressibility between the two isotopes shows the importance of nuclear quantum effects.



Confirmation of the Existence of the Widom Line !

